Photo- and electroproduction of nonstrange baryon resonances in the relativized quark model

Simon Capstick
Continuous Electron Beam Accelerator Facility, 12000 Jefferson Avenue, Newport News, Virginia 23606
(Received 19 May 1992)

Photoproduction amplitudes for the nonstrange baryons are calculated in a quark model with an electromagnetic transition operator containing relativistic corrections, and relativized-quark-model wave functions. A one-parameter fit to the photocouplings shows significant improvements over models using the nonrelativistic transition operator or nonrelativistic wave functions. Helicity asymmetries and other ratios in the electroproduction of some low-lying resonances are also predicted.

PACS number(s): 13.60.Rj, 12.40.Qq, 14.20.Gk

I. INTRODUCTION

The information contained in photoproduction amplitudes has been crucial to the development [1, 2] of the nonrelativistic quark potential model. The tables can be turned and the validity of spectral models which ultimately have arisen from this early work can be tested by examining their consequences for the baryon electromagnetic couplings. The best prospect for new data which can give further insight into the structure of baryons is from new and future experiments to measure these couplings, such as those at MIT/Bates and CEBAF. It is therefore of critical interest to compare the predictions of such models with the existing data.

Koniuk and Isgur [3] carried out such a systematic study of the effects of hyperfine mixing in baryon wave functions on the photocouplings, using a simple nonrelativistic electromagnetic transition operator. However Close and Li [4] argue that it is inconsistent to incorporate the effects of the hyperfine interaction on the wave function, which are $O(1/m^2)$, while using an $O(1/m)$ expansion of the transition operator. At $O(1/m^2)$ various new terms [4, 5] appear in the electromagnetic transition Hamiltonian; there are spin-orbit corrections, the accompanying two-body currents present in the three-body system, and dependence on the binding potential. Kubota and Ohta [6] studied one of these corrections, the spin-orbit term, using unmixed oscillator wave functions for the resonances, and found evidence for it in the photocoupling data.

The Koniuk-Isgur calculation was generalized by Sartor and Stancu [7], who studied the effects of using more realistic radial wave functions with the nonrelativistic operator, and Forsyth and Cutkosky [8] using a more general operator. Close and Li in Ref. [4] and Warns, Schröder, Pfeil, and Rollnik in Ref. [5] performed calculations with transition operators expanded consistently in p/m, and with Isgur-Karl model [9–11] wave functions for the resonances. However their treatment of excited P_{11} and P_{33} resonances was in error [12], due to the adoption of wave functions which are not orthogonal to the ground states $N(938)$ and $\Delta(1232)$. A more general issue is the effect of the truncation of the model space at the $N = 2$ band of the harmonic oscillator in the Isgur-Karl model. Furthermore, the energies of states are formed by diagonal perturbation theory in the anharmonic part of the potential; although these perturbations may be substantial, the effect on the wave functions is not included.

It is therefore of interest to calculate the electromagnetic couplings in a model which deals with the spin-independent potential in a more realistic way, such as the relativized model [13] as applied to baryons [14], and using a transition operator which includes the relativistic corrections in a consistent manner. The program outlined below has already been carried out (and the problems with orthogonality corrected) for the P_{11} and P_{33} resonances in Ref. [12]. Here this calculation is extended to other nonstrange baryons, and to electroproduction.

In the relativized model a generalized spectral Hamiltonian is solved in a large (to at least $N = 7$) harmonic oscillator basis. This Hamiltonian contains the usual spin-spin hyperfine interaction, treated in a different way, as well as spin-orbit energies; it also uses a minimum-length string confining potential (plus a color-Coulomb interaction at short distances) which yields an approximately linear potential between quarks. Potentials are allowed to become momentum dependent by, roughly speaking, replacing factors of quark mass with factors of quark energy. While the spectroscopy is of similar quality to that of the nonrelativistic model, in a model which is more tightly constrained, the resulting wave functions can be expected to be quite different from those of the nonrelativistic model, especially in their "radial" dependence.

The electromagnetic couplings of the nonstrange baryons, for both real- and virtual-photon excitation of resonances from the nucleon, are calculated here using these relativized-model wave functions, and the Close-Li transition operator. The signs of the photoexcitation amplitudes cannot be extracted from the data separately from the sign of the subsequent $N\pi$ decay of the resonance. Photoproduction amplitudes are therefore quoted [15] inclusive of this sign. There is also an extra conventional sign in the experimental amplitudes [15, 3]

of -1 $(+1)$ for the photoproduction of an N^* (Δ^*). References [7, 4, 5] adopt the $N\pi$ signs from Koniuk and Isgur [3], although Ref. [3] does not include a tabulation of the $N\pi$ signs for wave functions mixed by the hyperfine interaction. To avoid difficulties with sign conventions, etc., these signs are taken here from a quark-pair-creation ($^3P_0$) model calculation [16], which uses exactly the same (relativized-model) wave functions as input.

A simple fit to the photocouplings is carried out by varying the effective quark mass m^*, which should be thought of as the sum of the average kinetic energy and scalar-binding-potential energy [4] for a constituent quark in these states. Predictions are also made of the photocouplings of the "missing" states [17], baryon states present in the quark model but not in the $N\pi$ partial wave analyses, because of weak coupling [3] to $N\pi$. The relativized model also allows for the calculation of the photocouplings of states which first appear when the oscillator basis is extended [8] beyond $N = 2$; the photocouplings of the lowest-lying of these states are calculated.

Extension of these techniques to electroproduction amplitudes is a much more complicated task. The methods outlined above are inherently nonrelativistic, and while this may not present an insurmountable problem in the spectroscopy, in the calculation of transition amplitudes where momentum transfers of a few GeV^2 are involved, simple Galilean transformation of center-of-momentum frame wave functions (and the neglect of the small components of the quark spinors) becomes questionable. Constituent quarks should also be given electromagnetic form factors; however, relativistic effects in the transition matrix elements [18] and the treatment of the wave functions lead to Q^2 dependence which loosely resembles that of a (soft) quark form factor. This has led to the adoption [19] of very soft form factors for the quarks in the absence of a consistent treatment of relativistic effects. Other calculations [4, 5] adopt the approach of using size parameters in the nonrelativistic wave functions which can simulate such soft form factors, but which may not be consistent [9–11, 8, 14] with the values needed for a successful spectroscopy.

It is, however, still possible to make predictions for the Q^2 dependence of *ratios* of amplitudes, which are independent of many of these issues. In particular states X with total angular momentum $J_X \geq \frac{3}{2}$ can be excited from protons or neutrons with two different helicity combinations $(\lambda_N + \lambda_\gamma = -\frac{1}{2} \pm 1 = \lambda_X)$, and the helicity asymmetries $(A_{\frac{1}{2}}{}^2 - A_{\frac{3}{2}}{}^2)/(A_{\frac{1}{2}}{}^2 + A_{\frac{3}{2}}{}^2)$ can be formed. For states with $J = \frac{1}{2}$ it is also possible to reliably calculate $A^n_{\frac{1}{2}}/A^p_{\frac{1}{2}}$, or ratios of amplitudes with those of nearby states (since the neglected relativistic corrections will have similar effects for states nearby in energy and with similar spatial structure). Close and Gilman [20] correctly predicted that the helicity asymmetries of the $N\frac{3}{2}^-(1520)D_{13}$ and $N\frac{5}{2}^+(1680)F_{15}$ resonances would change rapidly with Q^2 if calculated with the nonrelativistic transition operator. These ratios have been studied by other authors in various models [21, 4, 5]; they are reexamined here, and other ratios predicted, with the model described above. The ratio E_{1+}/M_{1+} in the electroproduction of the $\Delta(1232)$ has also been extensively studied [22, 23], and has been examined in Ref. [24] using the relativized-model wave functions and the nonrelativistic transition operator; here this issue is reexamined using the transition Hamiltonian incorporating the Close-Li relativistic corrections.

This paper is organized as follows. The next section contains a summary of the new features of the relativized model used to generate the wave functions, and the electromagnetic transition Hamiltonian of Ref. [4] is rewritten in a form convenient for calculation in the basis in which they are expressed. This is followed by a section containing a description and discussion of the results for the photocouplings, and the results for amplitude ratios in electroproduction. The final section contains the conclusions which may be drawn. Details of the calculation of the matrix elements are included in an Appendix.

II. WAVE FUNCTIONS AND TRANSITION OPERATOR

A. Relativized-model wave functions

For a complete description of the relativized model see Refs. [13, 14]; here the main differences with the Isgur-Karl (nonrelativistic) model are outlined.

As in the nonrelativistic model the Schrödinger equation is solved in a Fock space made up of valence quarks. The Hamiltonian is given by

$$H = \sum_i \sqrt{\mathbf{p}_i^2 + m_i^2} + V, \tag{1}$$

where V is a relative-position and -momentum dependent potential which tends, in the nonrelativistic limit (*not* taken here), to

$$V \to V_{\text{string}} + V_{\text{Coul}} + V_{\text{hyp}} + V_{\text{so(cm)}} + V_{\text{so(Tp)}}. \tag{2}$$

Here V_{string} is the potential generated by adding the lengths of the gauge-invariant (Y-shaped) string configuration, and multiplying by the meson string tension $\sqrt{\sigma}$. The string is assumed to adjust instantaneously to the motion of the quarks so that it is always in its minimum length configuration; this generates a three-body adiabatic potential for the quarks [25] which includes genuine three-body forces. Here V_{Coul}, V_{hyp}, $V_{\text{so(cm)}}$, and $V_{\text{so(Tp)}}$ are color-Coulomb, color-hyperfine, color-magnetic spin-orbit, and Thomas-precession spin-orbit potentials. The color-Coulomb and hyperfine potentials are as in the nonrelativistic model [9, 10], except that the interquark coordinate $\mathbf{r}_{ij}$ is smeared out over mass-dependent distances, as suggested by relativistic kinematics and QCD, and the momentum dependence away from the $p/m \to 0$ limit is parametrized, as suggested by relativistic dynamics.

In practice this smearing is brought about by convoluting the potentials with a function

$$\rho_{ij}(\mathbf{r}_{ij}) = \frac{\sigma_{ij}^3}{\pi^{\frac{3}{2}}} e^{-\sigma_{ij}^2 r_{ij}^2}. \tag{3}$$

The σ_{ij} are chosen to smear the interquark coordinate over distances of $O(1/M_Q)$ for Q heavy, and approximately 0.1 fm for light quarks. The potentials are made momentum dependent by introducing factors which replace m_i where it appears in the nonrelativistic limit by, roughly, E_i. For example the contact part of $V_{\rm hyp}$ becomes $V_{\rm hyp} = \sum_{i<j} V^{ij}_{\rm cont}$, with

$$V^{ij}_{\rm cont} = \left(\frac{m_i m_j}{E_i E_j}\right)^{\frac{1}{2}+\epsilon_{\rm cont}} \frac{16\pi}{9}\alpha_s(r_{ij})\frac{\mathbf{S}_i\cdot\mathbf{S}_j}{m_i m_j}\left[\frac{\sigma_{ij}^3}{\pi^{\frac{3}{2}}}e^{-\sigma_{ij}^2 r_{ij}^2}\right]\left(\frac{m_i m_j}{E_i E_j}\right)^{\frac{1}{2}+\epsilon_{\rm cont}}. \tag{4}$$

Here $\epsilon_{\rm cont}$ is a constant parameter, and $\alpha_s(r_{ij})$ is a running-coupling constant which runs according to the lowest-order QCD formula, saturating to 0.6 at $Q^2 = 0$.

The color-magnetic and Thomas-precession spin-orbit potentials are also smeared and allowed to depend on momentum in a similar way; they also tend, in the nonrelativistic limit, to the spin-orbit potentials which are calculated (but not included) in the Isgur-Karl model. Their addition in the nonrelativistic model tends to spoil the agreement of the model with the experimental spectrum [9], especially that of the negative-parity P-wave states. This is not the case in the relativized model [14].

Nonstrange baryon states are then written as

$$\Psi = C_A\phi\sum\psi\chi, \tag{5}$$

where C_A is a totally antisymmetric (under the exchange group S_3) color wave function, ϕ is the flavor wave function uud or ddu, and the sum is performed so that the result is symmetric under exchange of quarks 1 and 2. The quark-spin states χ are the usual spin wave functions of total spin $\frac{1}{2}$ or $\frac{3}{2}$ formed from three spins $\frac{1}{2}$; for a given total J and parity P the individual terms $\psi\chi$ are implicitly L-S coupled. The spatial wave functions ψ are made up of solutions of the two three-dimensional oscillators

$$\psi_{LMn_\rho l_\rho n_\lambda l_\lambda} = \sum_m C(l_\rho, l_\lambda, m, M-m; L, M)|n_\rho\, l_\rho\, m\rangle|n_\lambda\, l_\lambda\, M-m\rangle, \tag{6}$$

where

$$|n_\rho\, l_\rho\, m\rangle = \mathcal{N}_{n_\rho l_\rho}\alpha^{\frac{3}{2}}(\alpha\rho)^{l_\rho}e^{-\frac{1}{2}\alpha^2\rho^2}L_{n_\rho}^{l_\rho+\frac{1}{2}}(\alpha^2\rho^2)Y_{l_\rho m}(\Omega_\rho), \tag{7}$$

and similarly for $|n_\lambda\, l_\lambda\, M-m\rangle$, and where $\mathcal{N}_{nl} = \sqrt{2n!/\Gamma(n+l+\frac{3}{2})}$.

The wave functions of baryon states with total spin and parity J^P can be expanded in a basis of (implicitly L-S coupled) states $\psi\chi$; the energies and wave functions of the baryon states are then formed by diagonalizing the Hamiltonian H in this basis. Note that the basis mixes nucleon ($I = \frac{1}{2}$) and delta ($I = \frac{3}{2}$) states; the $m_u = m_d$ symmetry of H ensures that the resulting eigenvectors are either delta states (with linear combinations $\sum\psi\chi$ totally symmetric under S_3) or nucleons (with mixed-λ symmetry). The basis extends to $N = 6$ for positive-parity states [26] and $N = 7$ for negative-parity states, where $N = 2(n_\rho+n_\lambda)+l_\rho+l_\lambda$, giving of the order of 100 substates [even under (12) exchange] for each J^P. Energies are minimized, state by state, by coarse variation of the oscillator size parameter α; however, in a calculation of transition amplitudes it is necessary to have all states expanded with the same α for orthogonality. A measure of the convergence of the expansion is the α dependence of these amplitudes, which will be discussed later.

The resulting spectroscopy is comparable to that of the Isgur-Karl model, with some improvements and some deterioration. This is a nontrivial test, as the model is much more tightly constrained; various quantities which were fit in the Isgur-Karl model (such as band centers of mass) are now predicted, and the same set of parameters [27] fits *all* mesons and baryons. Spin-orbit interactions are small but not neglected in this model; this is mainly due to the use of a smaller α_s, although there is, as expected, a partial cancellation of the color-magnetic and Thomas-precession spin-orbit terms, and the spin-orbit interactions are suppressed relative to the hyperfine contact term by the choice of $\epsilon_{\rm cont} < \epsilon_{\rm so}$. This smaller α_s yields the same contact splittings when the smeared contact interaction of Eq. (4) is evaluated without resorting to wave function perturbation theory (apart from basis truncation beyond $N = 6$).

The wave functions which result from this process differ substantially from those of the Isgur-Karl model. In the Isgur-Karl model the effects of the anharmonic terms are not included in the wave functions, even though the pattern of the mass splittings of the positive-parity excited states [10] is mainly driven by the anharmonicity, and the effects on the wave functions can be expected to be large (the splittings are comparable to the oscillator excitation energy ω). Since a nonsingular contact interaction with a smaller α_s is used, and all of the spin-dependent interactions are evaluated more precisely, we can also expect differences in the configuration mixings in the wave functions which they cause.

A simple test of the validity of this approach to baryon structure is to examine the electromagnetic transition amplitudes which result from calculation with these wave functions. This should be done with a transition opera-

tor which includes relativistic corrections in a consistent manner, such as that of Close and Li [4]. Details of this operator, and its calculation in the relativized model basis, are given next.

B. Transition operator

The nonrelativistic transition operator mentioned above is an $O(p/m)$ expansion of the expectation of the electromagnetic current between a pair of quark spinors:

$$H^{\rm nr} = -\sum_{i=1}^{3}\left\{\frac{e_i}{2m}\left(\mathbf{p}_i\cdot\mathbf{A}_i+\mathbf{A}_i\cdot\mathbf{p}_i\right)+\mu_i\boldsymbol{\sigma}_i\cdot\mathbf{B}_i\right\}, \quad (8)$$

where $m = m_u = m_d$ is the constituent quark mass, e_i, $\boldsymbol{\sigma}_i/2$, and $\mu_i = ge_i/2m$ are the charge, spin, and magnetic moment of the quark i, and $\mathbf{A}_i \equiv \mathbf{A}(\mathbf{r}_i)$. At order $(p/m)^2$ spin-orbit [28, 6] and two-body [28, 29, 4] terms must be added to these orbit-flip (convection) and spin-flip terms. At this order there is also dependence of the transition operator on the binding potential. Close and Li avoid explicit dependence on the vector-exchange part of the binding potential [30, 4] by rewriting the convection term; similarly by formally including kinetic and scalar-binding energies in the effective quark mass m^* the (equivalent to) scalar-exchange binding potential can be removed from the transition operator. The result is

$$H^{\rm em} = \sum_{i=1}^{3}\Bigg\{ -e_i\mathbf{r}_i\cdot\mathbf{E}_i + i\frac{e_i}{2m^*}\left(\mathbf{p}_i\cdot\mathbf{k}_i\mathbf{r}_i\cdot\mathbf{A}_i+\mathbf{r}_i\cdot\mathbf{A}_i\mathbf{p}_i\cdot\mathbf{k}_i\right)-\mu_i\boldsymbol{\sigma}_i\cdot\mathbf{B}_i$$
$$-\frac{1}{2m^*}\left(2\mu_i-\frac{e_i}{2m^*}\right)\frac{\boldsymbol{\sigma}_i}{2}\cdot\left[\mathbf{E}_i\times\mathbf{p}_i-\mathbf{p}_i\times\mathbf{E}_i\right]\Bigg\}+\sum_{i<j}\frac{1}{2M_Tm^*}\left(\frac{\boldsymbol{\sigma}_i}{2}-\frac{\boldsymbol{\sigma}_j}{2}\right)\cdot\left[e_j\mathbf{E}_j\times\mathbf{p}_i-e_i\mathbf{E}_i\times\mathbf{p}_j\right], \quad (9)$$

with M_T the recoil mass of the baryon system. Since the hyperfine interaction is itself of $O(p/m)^2$ the spin-orbit term should be included in a calculation which includes the hyperfine configuration mixings. The spin-orbit and two-body terms must both be included to have gauge invariance, and they are also necessary [28] if the electromagnetic interaction is to satisfy the low-energy theorems in Compton scattering, and the Drell-Hearn-Gerasimov sum rule.

In order to calculate the matrix elements of the components of Eq. (9), it is useful to write the transition operators to be used between the quark-model basis states in a form different from those of Ref. [4]. By insertion of the usual radiation field for the absorption of a photon into Eq. (9), and then integrating over the baryon center-of-mass coordinate, the transverse photoexcitation amplitudes can be written as simple expectation values over flavor, spin, and spatial internal coordinates

$$A_\lambda^N = \sum_{i=1}^{3}\langle X;J\lambda|H_i|N;\tfrac{1}{2}\lambda-1\rangle. \quad (10)$$

Here the initial photon has a momentum $\mathbf{k}\|\hat{\mathbf{z}}$, the initial nucleon has a momentum $\mathbf{P}_i\|\hat{\mathbf{z}}$, and the angular momenta are quantized along $\hat{\mathbf{z}}$. As the basis states described above (excluding the color wave function) are not totally exchange symmetric, the usual simplification of replacing a sum over quarks with three times the third-quark expectation value cannot be applied here. However, a simple procedure, that of transforming the wave functions to a basis which has redefined Jacobi coordinates, allows the calculation of the matrix elements of the H_1 and H_2 operators to proceed in an exactly similar way to that of the operator H_3. Calculation of the matrix elements of H_3 avoids complicated functions of the relative coordinates in the "recoil" exponential. The details of this procedure are outlined in Appendix A, and only third-quark operators are described here.

The operator H_3 can be written in the form

$$H_3 = H_3^{\rm nr} + H_3^{\rm vp} + H_3^{\rm so} + H_{12}^{\rm 2b}, \quad (11)$$

with the nonrelativistic (nr) operator

$$H_3^{\rm nr} = -\frac{e_3}{m^*}\frac{1}{\sqrt{2}}\sqrt{\frac{2\pi}{k_0}}\left(\sqrt{\frac{2}{3}}p_{\lambda+}-gk\frac{\sigma_{3+}}{2}\right)e^{-ik\sqrt{\frac{2}{3}}\lambda_z}. \quad (12)$$

Here k_0 is the 0 component of the photon four-momentum (equal to $k = |\mathbf{k}|$ for real photons), and the momenta $\mathbf{p}_\rho$ and $\mathbf{p}_\lambda$ are conjugate to the Jacobi three-body coordinates $\boldsymbol{\rho} = (\mathbf{r}_1-\mathbf{r}_2)/\sqrt{2}$ and $\boldsymbol{\lambda} = (\mathbf{r}_1+\mathbf{r}_2-2\mathbf{r}_3)/\sqrt{6}$. The derivative operator arises from the usual convection Hamiltonian

$$H^{\rm conv} = -\sum_{i=1}^{3}\frac{e_i}{2m^*}\left(\mathbf{p}_i\cdot\mathbf{A}_i+\mathbf{A}_i\cdot\mathbf{p}_i\right). \quad (13)$$

The difference $H^{\rm vp}$ between the rewritten convection term [the first two terms in Eq. (9)] and $H^{\rm conv}$ is a relativistic correction to the transition Hamiltonian due to the presence of the vector-exchange part of the binding potential; it can be written in the form

$$H_3^{\rm vp} = e_3\sqrt{\frac{2\pi}{k_0}}\sqrt{\frac{2}{3}}\left\{\left(\frac{-i}{\sqrt{2}}\lambda_+\right)\left[k_0+\frac{k}{m^*}\left(\sqrt{\frac{2}{3}}p_{\lambda z}+\frac{k}{6}-\frac{P_i}{3}\right)\right]-\frac{1}{m^*}\left(\frac{-p_{\lambda+}}{\sqrt{2}}\right)\right\}e^{-ik\sqrt{\frac{2}{3}}\lambda_z}, \tag{14}$$

where $P_i = |\mathbf{P}_i|$. Similarly the spin-orbit (so) operator may be written

$$H_3^{\rm so} = (2g-1)\frac{e_3}{2m^{*2}}\sqrt{\pi k_0}\left\{\frac{\sigma_{3+}}{2}\left(\sqrt{\frac{2}{3}}p_{\lambda z}+\frac{k}{6}-\frac{P_i}{3}\right)-\frac{\sigma_{3z}}{2}\sqrt{\frac{2}{3}}p_{\lambda+}\right\}e^{-ik\sqrt{\frac{2}{3}}\lambda_z}, \tag{15}$$

and the two-body (2b) operator has the form

$$H_{12}^{\rm 2b} = \frac{e_3}{2M_T m^*}\sqrt{\pi k_0}\left\{\frac{\sigma_{\rho+}}{2}p_{\rho z}-\frac{\sigma_{\rho z}}{2}p_{\rho+}+\frac{\sigma_{\lambda+}}{2}\left(p_{\lambda z}+\sqrt{\frac{2}{3}}[k+P_i]\right)-\frac{\sigma_{\lambda z}}{2}p_{\lambda+}\right\}e^{-ik\sqrt{\frac{2}{3}}\lambda_z}, \tag{16}$$

where $\boldsymbol{\sigma}_\rho = (\boldsymbol{\sigma}_1-\boldsymbol{\sigma}_2)/\sqrt{2}$, and $\boldsymbol{\sigma}_\lambda = (\boldsymbol{\sigma}_1+\boldsymbol{\sigma}_2-2\boldsymbol{\sigma}_3)/\sqrt{6}$.

The electromagnetic amplitudes calculated with these operators are frame dependent, even in the absence of the relativistic corrections of Eqs. (14), (15), and (16), which explicitly depend on P_i. The simple dependence of the operators on $k = |\mathbf{k}|$ (nonrelativistic kinematics) means that even the amplitudes calculated with Eq. (12) are frame dependent. In the next section a comparison of photocouplings calculated in the center-of-momentum (c.m.) frame (where $P_i = -k$) and in the Breit (Br) frame (where $P_i = -k/2$) is made, in order to estimate the error introduced by this lack of relativistic invariance. Although the amplitudes arising from individual relativistic corrections can be strongly frame dependent, this dependence becomes much weaker once their sum is formed [4, 12]. The Breit-frame calculation is theoretically preferable, and accordingly the results for photocouplings and electroproduction ratios are given in this frame. For photoproduction we have

$$k_0 = k = \begin{cases} \frac{M_X^2-M_N^2}{2M_X} & \text{c.m. frame,} \\ \frac{M_X^2-M_N^2}{\sqrt{2(M_X^2+M_N^2)}} & \text{Breit frame,} \end{cases} \tag{17}$$

and, for electroproduction in the Breit frame,

$$k^2 = \frac{(Q^2+M_X^2+M_N^2)^2-4M_X^2M_N^2}{Q^2+2(M_X^2+M_N^2)}, \tag{18}$$

$$k_0 = \sqrt{M_X^2+\frac{k^2}{4}}-\sqrt{M_N^2+\frac{k^2}{4}},$$

where $Q^2 = -(k_0^2-k^2)$. Note that the photon wave function normalization $\sqrt{2\pi/k_0}$ is well defined in the Breit frame (k_0 is never zero), although formally the choice of this normalization does not affect the amplitude ratios considered here.

III. PHOTOCOUPLINGS

A. Fit to photocouplings data

The process of relativization, as described above for the spectral Hamiltonian, parametrizes the momentum dependence away from the nonrelativistic limit by replacing factors of quark mass by factors of quark energy, and introduces quark smearing [Eq. (3)]. The momentum-dependence parameters of Refs. [13, 14] were determined by fitting the calculations to the wealth of data available for meson and baryon spectra. A less complicated procedure is adopted here, given the quality of the data. For the photocouplings of states made up of light quarks, and states which are not highly excited, it should be a reasonable approximation to replace the quark kinetic energy by a constant effective mass m^*. This effective mass was formally taken, in the expansion of Ref. [4], to include kinetic energy terms, along with an average scalar-binding-potential energy.

The effect of the quark smearing on the amplitudes is to multiply them by a nonrelativistic form factor which falls off as a function of the three-momentum transfer. If the light quarks are smeared as in Eq. (3), the result is a Gaussian quark form factor which decreases only a few percent over the range of momentum transfers considered here. This will have little effect on the photocouplings, and cannot affect ratios in electroproduction, and is therefore neglected.

The photocouplings are then fit by varying a single parameter, the effective quark mass m^* in Eq. (9). The ratio g/m^* is kept constant to maintain a simple additive explanation of the nucleon magnetic moments, and the recoil mass is kept at $M_T = 3m^*$. Using this procedure it is found that a modest increase (thirty percent) in the effective quark mass m^* significantly improves the fit to the measured photocouplings. A useful measure of the quality of the fit is to form a χ^2 statistic in the usual way [31] for the forty-six measured photocouplings [15]. Introducing a "theoretical error" avoids overemphasis in the fitting procedure of a few very well-measured photocouplings.

If, following Koniuk and Isgur [3], the photocouplings are calculated in the Breit frame with the nonrelativistic Hamiltonian of Eq. (8), Isgur-Karl model [9–12] wave functions with $\alpha = 0.41$ GeV, and $m = 0.336$ GeV ($g = 1$), a χ^2 of about 132 results. Here, and in all that follows, the signs of the photocoupling amplitudes for a particular set of wave functions are obtained by using those wave functions in a $^3P_0$ (quark-pair-creation) model strong decay calculation [16], and extracting the sign of the $X \to N\pi$ decay amplitude. Also for each

quark-model state the decay momentum is calculated with Eq. (17) from the experimental mass of the state for which it is the analogue. Adding the relativistic corrections $H^{\rm vp}$, $H^{\rm so}$, and $H^{\rm 2b}$ significantly lowers [4] χ^2 to 103; most of this improvement comes from adding the spin-orbit term [6]. If the effective quark mass m^* is increased thirty percent to 0.437 GeV (with corresponding $g = 1.3$ and $M_T = 3m^*$ GeV), χ^2 is improved to 89.

A further improvement is obtained when the Breit-frame photocouplings (and strong-decay signs) are calculated with the relativized-model wave functions. Using wave functions expanded in a basis with harmonic-oscillator $\alpha = 0.5$ GeV, the relativistic corrections once again improve the fit to the photocouplings, and the same modest increase in m^* lowers [32] χ^2 to 71. If the same calculation is performed using a basis with $\alpha = 0.6$ GeV, χ^2 rises by only 2.5, which demonstrates the soft dependence of the calculation on the intrinsic size of the basis used to expand the wave functions. Calculating in the center-of-momentum frame results in a χ^2 which is larger by 1.0 than that of the Breit-frame calculation. This illustrates that although the individual terms in the sum in Eq. (11) may be strongly frame dependent, their sum is not [4, 12].

The Breit-frame photocouplings calculated with the relativized-model wave functions for the ground state $\Delta(1232)$ and the low-lying (N=1 band) negative-parity baryons are shown in Table I. The results are shown decomposed into the pieces from $H^{\rm nr}$ (which is expressed as the sum of two terms: the convection term and the spin-flip term), $H^{\rm vp}$, $H^{\rm so}$, and $H^{\rm 2b}$. Table II shows the photocouplings for those of the positive-parity excited states in the $N = 2$ band for which there exist data. These results are summarized in Figs. 1 and 2. Here we have plotted, along with the data, the predicted Breit-frame photocouplings from three models: the calculation with Isgur-Karl wave functions with $\alpha = 0.41$ GeV, and the nonrelativistic transition operator with $m = 0.336$ GeV ($g = 1$), following Koniuk and Isgur; results for the same wave functions and parameters but with the relativistic corrections added, following the Close-Li A_1^M calculation; and results including all of the relativistic corrections with $m^* = 0.437$ GeV (and corresponding $g = 1.3$ and $M_T = 3m^*$), and using $\alpha = 0.5$ GeV relativized-model wave functions.

As a test of the procedure used to calculate these amplitudes and the $N\pi$ signs attached to them, the calculation of Ref. [4] has been reproduced for unmixed Isgur-Karl model wave functions in the center-of-momentum frame. The results [for all terms in Eq. (11)] agree in magnitude for all states. The overall multiplicative signs agree for all but $N\frac{1}{2}^+(1710)$, $N\frac{3}{2}^+(1720)$, $\Delta\frac{3}{2}^+(1600)$, and $\Delta\frac{3}{2}^+(1920)$. The sign of the Roper resonance $N\frac{1}{2}^+(1440)$ photocouplings also differs from Koniuk and Isgur (in agreement with Ref. [4]). In Koniuk and Isgur [3] the signs of the $N(1440)$, $N(1710)$, and $\Delta(1600)$ amplitudes were fixed by choosing the sign of a reduced amplitude P_0' in the strong decay analysis to fit the photocoupling data for the Roper resonance. In Ref. [16] there is no such freedom and the signs are predicted. The result of the different overall sign of the $N(1720)$ amplitude (which agrees with that predicted by Kubota and Ohta [6]) is to bring the calculations of Refs. [3, 7, 4] in closer agreement with the data.

In the $^3P_0$ model of Ref. [16] only the signs of the $N\pi$ amplitudes of two of these states, $\Delta\frac{3}{2}^+(1600)$ and $\Delta\frac{1}{2}^-(1620)$, are sensitive to mixings. When the Isgur-Karl wave functions are hyperfine mixed these signs both change, and they both change back when the fully mixed relativized-model wave functions are used, as can be seen in Figs. 1 and 2. In light of this sensitivity, the signs from the relativized-model wave functions may be the most trustworthy, as this model allows the initial and final wave functions the most freedom to mix *via* the interactions.

From the individual contributions to χ^2 from each resonance photocoupling listed in Tables I and II we can see that one-third of the χ^2 arises from the photocouplings of the lightest two states, $\Delta(1232)$ and the Roper resonance $N(1440)$. The discrepancy between the Roper resonance photocouplings calculated in this kind of model and the data has been noted by many authors; their work is referred to, and this issue discussed, in Ref. [12]. It is significant that these states are both light and couple strongly to πN; it is possible that pion loop effects (neglected here) renormalize their couplings [33]. It is also possible that the discrepancy is due to our lack of understanding of the relation between our model predictions and the resonance photocouplings extracted from the single-pion photoproduction partial-wave analyses [34].

Other states which have large contributions to χ^2 are the S_{31} state $\Delta(1620)$ (with $J^P = \frac{1}{2}^-$), the P_{33} state $\Delta(1600)$ (with $J^P = \frac{3}{2}^+$), which is discussed in Ref. [12], and the F_{15} $N(1680)$ (with $J^P = \frac{5}{2}^+$). In the case of the latter state only the $A^p_{\frac{3}{2}}$ amplitude seems in error. Although it is tempting to blame this discrepancy on a large $H^{\rm vp}$ correction (which has been verified analytically) the overall fit to the data is not significantly degraded by the addition of these vector-potential terms, which must be present for theoretical consistency [30, 4]. The expectation value of the $H^{\rm vp}$ term for this $A^p_{\frac{3}{2}}$ transition is strongly dependent on the oscillator-size parameter α due to a cancellation.

B. Missing resonances

Baryon states exist in the quark model for which there are, as yet, no experimental analogues. In particular there are eleven nucleon and delta states in the $N = 2$ band which are not seen in the single-pion photoproduction partial-wave analyses, and not seen (or not confirmed) in the $N\pi$ analyses. In their strong decay calculation, Koniuk and Isgur [3] found a natural explanation for this: states which are present in the $N\pi$ analyses correspond, in both energy and number, to states in the quark model which couple relatively strongly to the $N\pi$ channel. The missing states have weaker couplings. The examination of multipion final states (such as $\Delta\pi$,

TABLE I. Breit-frame photoproduction amplitudes using the $\alpha = 0.5$ GeV relativized-model wave functions of Ref. [14] and the operators $H_{\rm nr}$, $H^{\rm vp}$, $H_{\rm so}$, and $H_{\rm 2b}$. Here $m^* = 437$ MeV ($g = 1.3$ and $M_T = 3m^*$). Amplitudes are in units of 10^{-3} GeV$^{-\frac{1}{2}}$; a factor of $+i$ is suppressed for all negative-parity states.

State	A^N_λ	$A_{\rm nr}$	$A_{\rm vp}$	$A_{\rm so}$	$A_{\rm 2b}$	Total	Expt.	χ^2
$\Delta\frac{3}{2}^+(1232)$	$A^{p,n}_{\frac{1}{2}}$	0−107	0	−2	0	−108	−141±5	2.6
	$A^{p,n}_{\frac{3}{2}}$	0−185	0	−1	1	−186	−258±19	6.7
$N\frac{1}{2}^-(1535)$	$A^{p}_{\frac{1}{2}}$	92+65	−18	−97	34	76	73±14	0.0
	$A^{n}_{\frac{1}{2}}$	−94−30	18	42	0	−63	−76±32	0.1
$N\frac{1}{2}^-(1650)$	$A^{p}_{\frac{1}{2}}$	28+25	−6	−29	35	54	48±16	0.0
	$A^{n}_{\frac{1}{2}}$	−28+14	6	−27	0	−35	−17±37	0.2
$\Delta\frac{1}{2}^-(1620)$	$A^{p,n}_{\frac{1}{2}}$	90−26	−17	33	0	81	19±16	5.9
$N\frac{3}{2}^-(1520)$	$A^{p}_{\frac{1}{2}}$	67−91	−14	32	−8	−15	−22±10	0.1
	$A^{n}_{\frac{1}{2}}$	−68+35	14	−19	0	−38	−65±13	1.3
	$A^{p}_{\frac{3}{2}}$	116−1	−24	57	−15	134	167±10	2.2
	$A^{n}_{\frac{3}{2}}$	−118+13	24	−33	0	−114	−144±14	1.5
$N\frac{3}{2}^-(1700)$	$A^{p}_{\frac{1}{2}}$	15−30	−1	12	−28	−33	−22±12	0.2
	$A^{n}_{\frac{1}{2}}$	−15−1	2	34	−1	18	0±56	0.1
	$A^{p}_{\frac{3}{2}}$	25+6	2	22	−49	−3	0±19	0.0
	$A^{n}_{\frac{3}{2}}$	−26−64	3	57	0	−30	−2±44	0.3
$\Delta\frac{3}{2}^-(1700)$	$A^{p,n}_{\frac{1}{2}}$	58+42	−6	−12	0	82	116±17	1.7
	$A^{p,n}_{\frac{3}{2}}$	100−1	−10	−21	0	68	77±28	0.1
$N\frac{5}{2}^-(1675)$	$A^{p}_{\frac{1}{2}}$	1+3	−1	−1	0	2	19±12	0.6
	$A^{n}_{\frac{1}{2}}$	0−35	1	−1	0	−35	−47±23	0.1
	$A^{p}_{\frac{3}{2}}$	−1+3	1	0	0	3	19±12	0.4
	$A^{n}_{\frac{3}{2}}$	0−50	0	−1	0	−51	−69±19	0.4

TABLE II. Breit-frame photoproduction amplitudes for positive-parity ($N = 2$ band) excited states for which there exist data. Caption as in Table I.

State	A_λ^N	$A_{\rm nr}$	$A_{\rm vp}$	$A_{\rm so}$	$A_{\rm 2b}$	Total	Expt.	χ^2
$N\frac{1}{2}^+(1440)$	$A^p_{\frac{1}{2}}$	0+31	0	−33	6	4	−69±7	11.9
	$A^n_{\frac{1}{2}}$	0−20	0	20	−6	−6	37±19	2.5
$N\frac{1}{2}^+(1710)$	$A^p_{\frac{1}{2}}$	1+32	0	−22	1	13	5±16	0.1
	$A^n_{\frac{1}{2}}$	0−16	0	8	−2	−11	−5±23	0.0
$\Delta\frac{1}{2}^+(1910)$	$A^{p,n}_{\frac{1}{2}}$	−1+21	0	−42	14	−8	−12±30	0.0
$N\frac{3}{2}^+(1720)$	$A^p_{\frac{1}{2}}$	59+53	−45	−94	15	−11	52±39	2.1
	$A^n_{\frac{1}{2}}$	−19−33	15	56	−16	4	−2±26	0.0
	$A^p_{\frac{3}{2}}$	−34−1	26	−23	1	−31	−35±24	0.0
	$A^n_{\frac{3}{2}}$	11+1	−9	9	−1	11	−43±94	0.3
$\Delta\frac{3}{2}^+(1600)$	$A^{p,n}_{\frac{1}{2}}$	0+41	0	−15	5	30	−22±29	2.2
	$A^{p,n}_{\frac{3}{2}}$	0+71	0	−28	8	51	1±22	2.8
$\Delta\frac{3}{2}^+(1920)$	$A^{p,n}_{\frac{1}{2}}$	−14+26	9	−23	14	13	40±30	0.6
	$A^{p,n}_{\frac{3}{2}}$	6−24	−5	50	−14	14	23±30	0.1
$N\frac{5}{2}^+(1680)$	$A^p_{\frac{1}{2}}$	49−62	−22	32	−2	−38	−17±10	0.0
	$A^n_{\frac{1}{2}}$	−16+34	13	−15	3	19	31±13	0.3
	$A^p_{\frac{3}{2}}$	69+0	−54	45	−4	56	127±12	9.4
	$A^n_{\frac{3}{2}}$	−22−3	19	−21	4	−23	−30±14	0.1
$\Delta\frac{5}{2}^+(1905)$	$A^{p,n}_{\frac{1}{2}}$	19+0	−13	20	−2	26	27±13	0.0
	$A^{p,n}_{\frac{3}{2}}$	28−38	−18	28	−2	−1	−47±19	2.7
$N\frac{7}{2}^+(1990)$	$A^p_{\frac{1}{2}}$	0−2	1	1	0	−1	24±30	0.5
	$A^n_{\frac{1}{2}}$	0−14	0	−1	0	−15	−49±45	0.5
	$A^p_{\frac{3}{2}}$	0−2	0	0	0	−2	31±55	0.3
	$A^n_{\frac{3}{2}}$	0−18	0	0	0	−18	−122±55	3.1

TABLE II. *(Continued).*

State	A_λ^N	$A_{\rm nr}$	$A_{\rm vp}$	$A_{\rm so}$	$A_{\rm 2b}$	Total	Expt.	χ^2
$\Delta\frac{7}{2}^+(1950)$	$A^{p,n}_{\frac{1}{2}}$	0–32	0	−1	0	−33	−73±14	2.7
	$A^{p,n}_{\frac{3}{2}}$	0–41	0	0	0	−42	−90±13	4.1

$N\rho$, and $N\omega$ [17]) in new photoproduction experiments at CEBAF may provide a means to access these states without invoking a factor of this small $N\pi$ coupling. Whether or not a missing resonance is seen in one of these processes (or perhaps in single-pion photoproduction) depends crucially on the strength of its photocouplings.

Table III shows these photocouplings for the missing states up to $N = 2$, calculated with the relativized-model wave functions and the transition operator of Eq. (9), and the parameters of the best fit above. Also listed are the order in which these states appear in their partial waves, and their model masses from Ref. [14]. The photocouplings of these missing states tend to be disappointingly small, as can be seen from a comparison of Tables II and III. This can be expected as part of a general trend towards weaker photocouplings as the mass (and hence degree of excitation) of the resonance increases; it is also true that the largest nonrelativistic photocouplings [17] tend to be reduced by the relativistic corrections. For example the $\Delta\frac{5}{2}^+(1990)[F_{35}]_2$ state has $A^p_{\frac{1}{2}} = -38$ and $A^p_{\frac{3}{2}} = -68$ (in units of $10^{-3}\,\mathrm{GeV}^{-\frac{1}{2}}$) when calculated with the nonrelativistic $H^{\rm nr}$, and these reduce to $A^p_{\frac{1}{2}} = -10$ and $A^p_{\frac{3}{2}} = -28$ when calculated with Eq. (9).

The situation is not, however, hopeless; there are states which are well established in single-pion photoproduction which have photocouplings smaller than those of some states in Table III. For example it may be possible to extract a signal for the lightest P_{31} state, $\Delta\frac{1}{2}^+(1835)$ in Ref. [14]. Also there is [15] a two-star experimental state $N(2000)F_{15}$ seen in $N\pi$ which may be one of the F_{15} quark-model states in Table III; the predicted photocouplings for these states are not negligibly small. The quark-model state $\Delta\frac{5}{2}^+(1990)[F_{35}]_2$ mentioned above [the analogue of the two-star state seen in $N\pi$, $\Delta(2000)F_{35}$] has photocouplings which are smaller than the nonrelativistic expectations but which may still allow its observation through one of the multipion final states above. Similarly one or both of the model states $N\frac{3}{2}^+(1870)[P_{13}]_2$ and $N\frac{3}{2}^+(1910)[P_{13}]_3$ may be visible, the former perhaps in pion photoproduction as it has [17, 16] an appreciable coupling to $N\pi$.

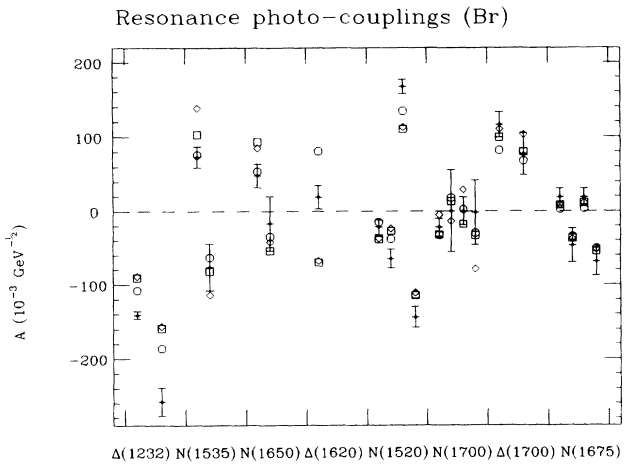

FIG. 1. Breit-frame photoproduction amplitudes for $\Delta(1232)$ and the P-wave resonances. Diamonds and squares are for calculations using Isgur-Karl wave functions with $\alpha = 0.41$ GeV, and $H^{\rm nr}$ and $H^{\rm em}$ respectively, with $m(m^*) = 0.336$ GeV, $g = 1$, and $M_T = 3m^*$; circles are the "total" amplitudes from Table I. For Δ states $A_{\frac{1}{2}}$ and $A_{\frac{3}{2}}$ (where allowed) amplitudes are displaced, with $A^{p,n}_{\frac{3}{2}}$ plotted to the right of the corresponding $A^{p,n}_{\frac{1}{2}}$. For N states with $J = \frac{1}{2}$, A^p and A^n amplitudes are displaced, with $A^n_{\frac{1}{2}}$ plotted to the right of $A^p_{\frac{1}{2}}$; similarly for N states with $J \geq \frac{3}{2}$ amplitudes are plotted, from left to right, in the order $A^p_{\frac{1}{2}}$, $A^n_{\frac{1}{2}}$, $A^p_{\frac{3}{2}}$, and $A^n_{\frac{3}{2}}$. Data points, taken from Ref. [15], are also plotted with error bars.

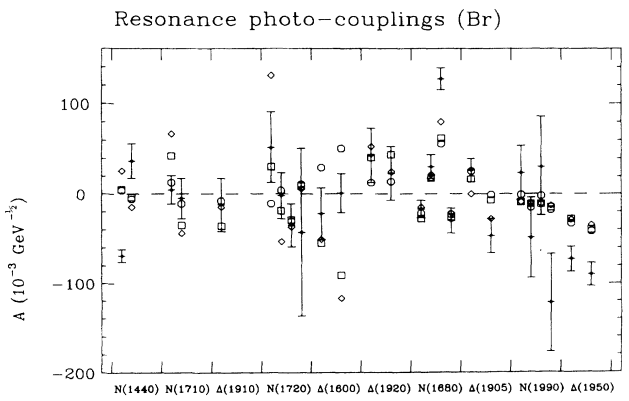

FIG. 2. Breit-frame photoproduction amplitudes for positive-parity excited ($N = 2$ band) states for which there exist data. Caption as in Fig. 1.

TABLE III. Breit-frame photoproduction amplitudes for "missing" positive-parity ($N = 2$ band) excited states, calculated using the $\alpha = 0.5$ GeV relativized-model wave functions of Ref. [14] and the full transition operator $H^{\rm em}$. Parameters and units are as in Table I, model masses are from Ref. [14]. $[F_{15}]_2$, e.g., is a notation for the second most-massive state in the F_{15} $N\pi$ partial wave. $A^p = A^n$ for Δ states.

State	$A^p_{\frac{1}{2}}$	$A^n_{\frac{1}{2}}$	$A^p_{\frac{3}{2}}$	$A^n_{\frac{3}{2}}$
$N\frac{1}{2}^+(1880)[P_{11}]_4$	0	−9		
$N\frac{1}{2}^+(1975)[P_{11}]_5$	−12	8		
$\Delta\frac{1}{2}^+(1835)[P_{31}]_1$	−31			
$N\frac{3}{2}^+(1870)[P_{13}]_2$	−2	14	−15	19
$N\frac{3}{2}^+(1910)[P_{13}]_3$	−21	10	−27	25
$N\frac{3}{2}^+(1950)[P_{13}]_4$	−5	−2	2	3
$N\frac{3}{2}^+(2030)[P_{13}]_5$	−9	6	15	−10
$\Delta\frac{3}{2}^+(1985)[P_{33}]_4$	6		3	
$N\frac{5}{2}^+(1980)[F_{15}]_2$	−11	22	−6	11
$N\frac{5}{2}^+(1995)[F_{15}]_3$	−18	−2	1	7
$\Delta\frac{5}{2}^+(1990)[F_{35}]_2$	−10		−28	

C. Other low-lying resonances

There are many well-established states in the $N\pi$ analyses which, by counting arguments, have as their quark-model analogues states which first appear in the $N = 3$ or $N = 4$ bands. The situation for the positive-parity $N = 4$ band excited states with relatively small total spin J is difficult, as there are already many lighter states in their partial waves, some of which are already "missing." However, this is not the case for some of the lighter states with higher J. In the case of the negative-parity $N = 3$ band excited states there are just one or two states in their partial waves at $N = 1$; there are several quite well established more massive ($N = 3$ band) states in the $N\pi$ analyses [15]. It is therefore of interest to examine the photocouplings of the low-lying $N = 3$ band excitations and some of the higher-J $N = 4$ band states in the model which best fits the known photocouplings above.

As there are many states which appear in these higher bands, and as the photocouplings tend to diminish as the degree of excitation increases, the calculation is limited to the first few states above the $N = 2$ band in each partial wave. These photocouplings are listed in Tables IV and V; as a rule of thumb only those states with at least one photocoupling at least as large as 10 (in units of 10^{-3} GeV$^{-\frac{1}{2}}$), or for which there are experimental analogues in $N\pi$, are tabulated. There are some (rather uncertain) photocoupling data for some of the negative-parity states, which are listed under the predictions for the quark-model state which is best assigned to the observed state (in the spectroscopic and strong decay models of Refs. [14] and [16]).

In Tables IV and V it is encouraging that the $N = 3$ band model states with the largest predicted photocouplings correspond to those states for which there are some data listed in Ref. [15]. It might be possible to improve the experimental situation for these higher band states, and provide serious constraints for models, by an analysis of new photoproduction data using single and multipion final states. It may also be possible to discover new $N = 3$ and $N = 4$ band states in such experiments, such as the model state $\Delta\frac{7}{2}^+(2370)[F_{37}]_1$, which essentially decouples [16] from $N\pi$.

IV. ELECTROPRODUCTION RATIOS

Despite problems with the treatment of relativistic effects in the boosting of the center-of-momentum frame wave functions, and in the treatment of the quark spinors, it is still possible to reliably predict the Q^2 dependence of certain *ratios* of amplitudes. These ratios should be largely independent of these difficulties when taken between amplitudes for exciting the same resonance from different targets or with different final helicities, or between amplitudes for states nearby in energy and with similar spatial structure. Problems in the treatment of light-meson degrees of freedom, which may be responsible for the discrepancies between the extracted photocouplings of certain states and the model predictions, should be less apparent at higher Q^2. Accordingly the helicity asymmetries $(A_{\frac{1}{2}}{}^2 - A_{\frac{3}{2}}{}^2)/(A_{\frac{1}{2}}{}^2 + A_{\frac{3}{2}}{}^2)$ for proton and neutron targets are predicted for negative-parity states in the $N = 1$ band and some low-lying positive-parity excited states, using the relativized model above which yields the best fit to the photocouplings data.

For negative-parity states with $J = \frac{1}{2}$, certain ratios between their helicity-$\frac{1}{2}$ amplitudes and those of nearby states are also predicted. For $J = \frac{1}{2}$ states it is also of interest to examine the Q^2 dependence of the ratio $A^n_{\frac{1}{2}}/A^p_{\frac{1}{2}}$. Calculations are all made in the Breit frame to minimize recoil effects. For comparative purposes ratios are also calculated with the following models: $H^{\rm nr}$ and pure-oscillator or hyperfine-mixed wave functions, to illustrate the changes brought about by mixing in the Isgur-Karl model [40]; and with mixed Isgur-Karl model wave functions and the corrected $H^{\rm em}$ (with $m^* = 0.336$ GeV, $g = 1$) following Close and Li, in order to see the effects of use of the relativized-model wave functions and the increased effective quark mass.

Most of the data for electroproduction of baryon resonances have been collected for $\Delta(1232)$ and a few of the lightest N^*'s. In the following a comparison is made between the calculation and the data for the helicity asymmetries of $N\frac{3}{2}^-(1520)$ and $N\frac{5}{2}^+(1680)$, and the ratio between the $A^p_{\frac{1}{2}}$ amplitudes for $N\frac{3}{2}^-(1520)$ and

TABLE IV. Breit-frame photoproduction amplitudes for some negative-parity $N = 3$ band and positive-parity $N = 4$ band excited nucleon states, calculated using the $\alpha = 0.5$ GeV relativized-model wave functions of Ref. [14] and the full transition operator $H^{\rm em}$. Parameters and units are as in Table I, model masses are from Ref. [14]. Data are from Ref. [15]; a factor of $+i$ is suppressed for all negative-parity states.

Model state	$N\pi$ state	$A^p_{\frac{1}{2}}$	$A^n_{\frac{1}{2}}$	$A^p_{\frac{3}{2}}$	$A^n_{\frac{3}{2}}$	Ref.
$N\frac{1}{2}^-(1945)[S_{11}]_3$	$N(2090)*$	12	−4			
$N\frac{1}{2}^-(2030)[S_{11}]_4$		20	−15			
$N\frac{3}{2}^-(1960)[D_{13}]_3$	$N(2080)**$	36	−3	−43	27	
		−20±8	7±13	17±11	−53±34	[35]
		26±52	53±83	128±57	100±141	[36]
$N\frac{3}{2}^-(2055)[D_{13}]_4$		16	−18	0	0	
$N\frac{3}{2}^-(2095)[D_{13}]_5$		−9	8	−14	1	
$N\frac{5}{2}^-(2080)[D_{15}]_2$		−3	−9	−14	−9	
$N\frac{5}{2}^-(2095)[D_{15}]_3$		−2	22	−6	29	
$N\frac{7}{2}^+(2390)[F_{17}]_2$		−14	5	−11	7	
$N\frac{7}{2}^+(2410)[F_{17}]_3$		1	−15	−1	18	
$N\frac{7}{2}^-(2090)[G_{17}]_1$	$N(2190)****$	−34	10	28	−14	
		−55	−42	81	−126	[37]
		−30	−85	180	7	[38]
$N\frac{7}{2}^-(2205)[G_{17}]_2$		−16	13	4	−10	
$N\frac{9}{2}^+(2345)[H_{19}]_1$	$N(2220)****$	−29	16	13	−8	
$N\frac{9}{2}^-(2215)[G_{19}]_1$		0	−14	1	−17	

$N\frac{1}{2}^-(1535)$. Electroproduction of the Roper resonance, which has poorly predicted photocouplings in this model, is compared to that of the $\Delta(1232)$.

A. $\Delta(1232)$

In the absence of the tensor part of the color-hyperfine interactions, which mixes D-wave components into the wave functions of $\Delta(1232)$ and $N(938)$, the nonrelativistic model predicts a pure M_{1+} transition between these two states. A nonzero E_{1+} transition amplitude can therefore be considered evidence of the existence of the tensor interactions. For this reason there has been much theoretical and experimental interest [22, 23] in the ratio $E_{1+}/M_{1+} = (\sqrt{3}A_{\frac{1}{2}} - A_{\frac{3}{2}})/(\sqrt{3}A_{\frac{1}{2}} + 3A_{\frac{3}{2}})$. Figure 3 illustrates the effect of inclusion of the relativistic corrections to $H^{\rm nr}$ on this ratio, which has been calculated with hyperfine-mixed Isgur-Karl wave functions, and the fully mixed relativized wave functions.

With the Isgur-Karl wave functions E_{1+}/M_{1+} is a rapidly increasing function of Q^2, with a value of -0.4% at the photon point [41] when the nonrelativistic $H^{\rm nr}$ is

TABLE V. Breit-frame photoproduction amplitudes for some negative-parity $N = 3$ band and positive-parity $N = 4$ band excited delta states. Caption as in Table IV.

Model state	$N\pi$ state	$A^{p,n}_{\frac{1}{2}}$	$A^{p,n}_{\frac{3}{2}}$	Ref.
$\Delta\frac{1}{2}^-(2035)[S_{31}]_2$	$\Delta(1900)***$	20		
		−4±16		[39]
		29±8		[35]
$\Delta\frac{1}{2}^-(2140)[S_{31}]_3$	$\Delta(2150)*$	4		
$\Delta\frac{3}{2}^-(2080)[D_{33}]_2$	$\Delta(1940)*$	−20	−6	
		−36±58	−31±12	[35]
$\Delta\frac{3}{2}^-(2145)[D_{33}]_3$		0	10	
$\Delta\frac{5}{2}^-(2155)[D_{35}]_1$	$\Delta(1930)***$	11	19	
		−30±40	−10±35	[15]
$\Delta\frac{7}{2}^+(2370)[F_{37}]_1$		−33	−42	
$\Delta\frac{7}{2}^+(2460)[F_{37}]_2$	$\Delta(2390)*$	24	30	
$\Delta\frac{7}{2}^-(2230)[G_{37}]_1$	$\Delta(2200)*$	14	−4	
$\Delta\frac{9}{2}^-(2295)[H_{39}]_1$	$\Delta(2400)**$	−14	−17	
$\Delta\frac{11}{2}^+(2450)[H_{3,11}]_1$	$\Delta(2420)****$	−13	−16	

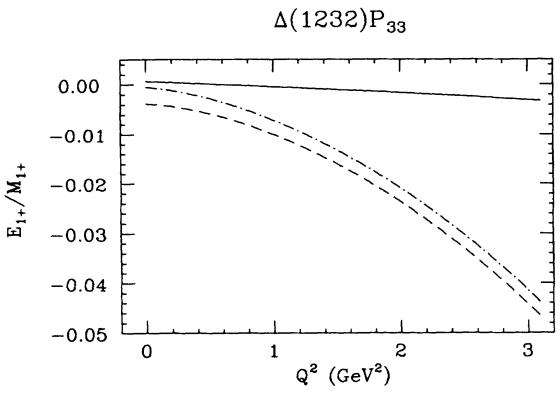

FIG. 3. Ratio E_{1+}/M_{1+} for electroproduction of $\Delta(1232)P_{33}$, calculated in the Breit frame. The dashed curve is calculated with mixed Isgur-Karl model wave functions ($\alpha = 0.41$ GeV) and $H^{\rm nr}$, the dashed-dotted curve with the same wave functions and the full $H^{\rm em}$, and the solid curve with the relativized-model wave functions ($\alpha = 0.5$ GeV) and $H^{\rm em}$ with $m^* = 0.437$ GeV ($g = 1.3$, $M_T = 3m^*$).

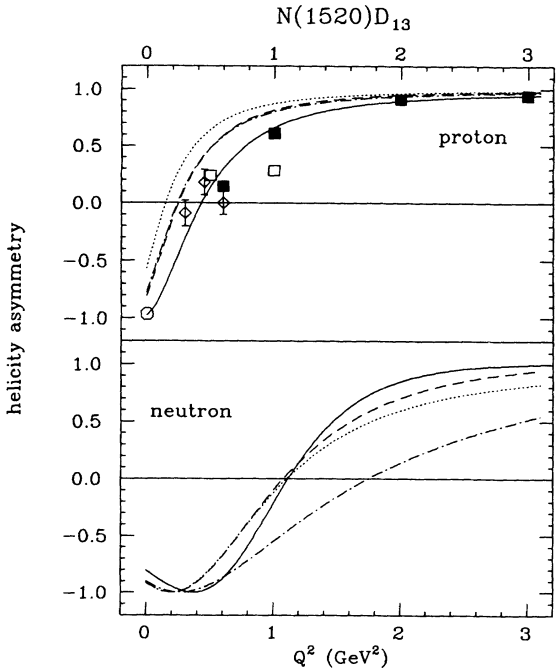

FIG. 4. Proton and neutron-target helicity asymmetries $(A_{\frac{1}{2}}{}^2 - A_{\frac{3}{2}}{}^2)/(A_{\frac{1}{2}}{}^2 + A_{\frac{3}{2}}{}^2)$ for electroproduction of $N(1520)D_{13}$, calculated in the Breit frame. The dotted and dashed curves are calculated with $H^{\rm nr}$ and unmixed- and mixed-oscillator wave functions ($\alpha = 0.41$ GeV), respectively, the dashed-dotted curve with mixed-oscillator wave functions and the full $H^{\rm em}$, and the solid curve with the relativized-model wave functions ($\alpha = 0.5$ GeV), and $H^{\rm em}$ with $m^* = 0.437$ GeV ($g = 1.3$, $M_T = 3m^*$). Experimental ratios from Burkert [42] with data from Ref. [15] ($Q^2 = 0$), Ref. [43] (diamonds), Ref. [44] (open squares), and Ref. [45] (solid squares).

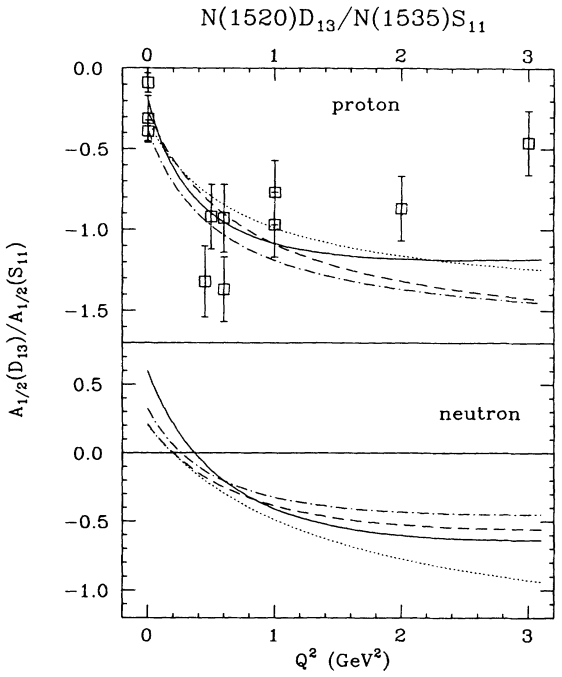

FIG. 5. Ratios of $A_{\frac{1}{2}}$ electroproduction amplitudes with proton and neutron targets for $N(1520)D_{13}/N(1535)S_{11}$, calculated in the Breit frame. Legend for the calculation as in Fig. 4; experimental ratios from Burkert [42] with data from Refs. [43–45].

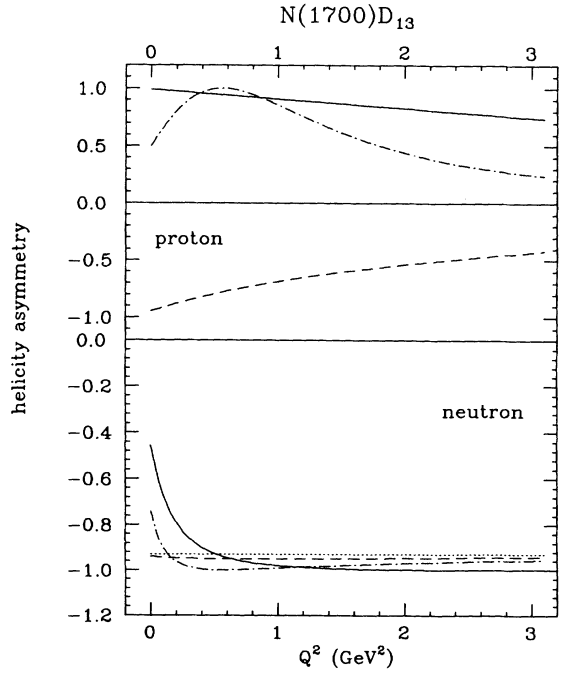

FIG. 6. Proton and neutron-target helicity asymmetries for electroproduction of $N(1700)D_{13}$, calculated in the Breit frame. Legend as in Fig. 4.

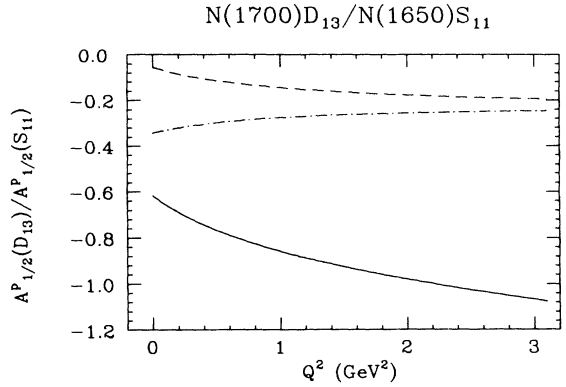

FIG. 7. Ratio of $A^p_{\frac{1}{2}}$ electroproduction amplitudes for $N(1700)D_{13}/N(1650)S_{11}$, calculated in the Breit frame. Legend as in Fig. 4.

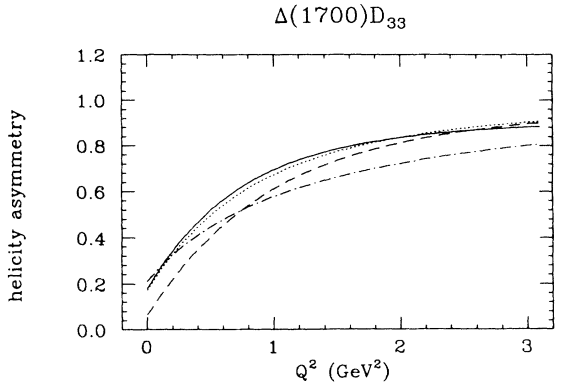

FIG. 9. Helicity asymmetry for electroproduction of $\Delta(1700)D_{33}$, calculated in the Breit frame. Legend as in Fig. 4.

used. However, inclusion of the relativistic corrections in Eq. (9) reduces the photon-point value to essentially zero, with the largest cancelling contribution coming from the spin-orbit term. Given the theoretical necessity for the spin-orbit term in Eq. (9), and the evidence for it in the fit to the photocouplings, it would appear that a nonzero E_{1+}/M_{1+} at the photon point cannot be attributed to hyperfine mixing. The behavior as a function of Q^2 is largely unchanged. When the calculation is made with the relativized-model wave functions and the corrected transition Hamiltonian, E_{1+}/M_{1+} remains small at $Q^2 = 0$ and develops very weak dependence on Q^2. This weak dependence with the relativized-model wave functions was found (with $H^{\rm nr}$) in Ref. [24]; the effect of the corrections to $H^{\rm nr}$ is to further reduce the ratio at higher Q^2. The experimental situation [23] for this ratio is too uncertain to distinguish between these (and other) models.

B. Negative-parity states

Figure 4 shows the helicity asymmetries $(A_{\frac{1}{2}}{}^2 - A_{\frac{3}{2}}{}^2)/(A_{\frac{1}{2}}{}^2 + A_{\frac{3}{2}}{}^2)$ for $N\frac{3}{2}^-(1520)$, with both proton and neutron targets. There is an obvious improvement in the agreement with the proton-target data when the nonrelativistic wave functions are mixed, and again as the relativized-model wave functions and larger m^* are used. The latter is not unexpected given the improved agreement with the photocouplings for this state evident in Table I. The neutron asymmetry is strongly affected by the addition of the relativistic corrections to $H^{\rm nr}$; it regains a Q^2 dependence similar to that of the nonrelativistic model when calculated in the relativized model.

The ratios between the $A_{\frac{1}{2}}$ amplitudes for $N\frac{3}{2}^-(1520)$ and $N\frac{1}{2}^-(1535)$ are plotted along with the proton-target data in Fig. 5. Although none of the curves appear to fit the data at the higher Q^2 values [1, 4], there is again an improvement with the relativized-model calculation. This is an instance where, as suggested by Close and Li, it appears that higher configurations in the QCD mixed wave functions become important.

Model predictions for the helicity asymmetries of the second D_{13} resonance $N\frac{3}{2}^-(1700)$ are shown in Fig. 6. The proton-target amplitudes are both zero when calculated with $H^{\rm nr}$ and unmixed-oscillator wave functions;

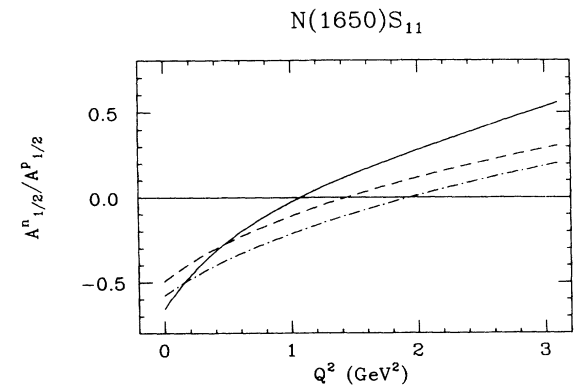

FIG. 8. Ratio $A^n_{\frac{1}{2}}/A^p_{\frac{1}{2}}$ for electroproduction of $N(1650)S_{11}$, calculated in the Breit frame. Legend as in Fig. 4.

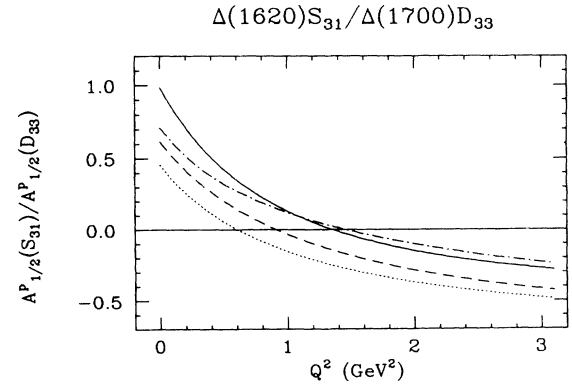

FIG. 10. Ratio of $A_{\frac{1}{2}}$ electroproduction amplitudes for $\Delta(1620)S_{31}/\Delta(1700)D_{33}$, calculated in the Breit frame. Legend as in Fig. 4.

hyperfine mixing gives a substantial $A^p_{\frac{3}{2}} \gg A^p_{\frac{1}{2}}$, and relativistic corrections reverse this to $A^p_{\frac{1}{2}} > A^p_{\frac{3}{2}}$. The relativized-model wave functions and smaller effective mass yield an $A^p_{\frac{1}{2}} \gg A^p_{\frac{3}{2}}$ for smaller Q^2. A precision measurement of this asymmetry, while difficult (the amplitudes are relatively small, see Table I), could easily test for the presence of hyperfine mixing and these relativistic corrections. For neutron targets the amplitudes rapidly settle into a ratio close to $-13/14$, the value obtained [in the "SU(6) limit"] using $H^{\rm nr}$, and without mixing in the wave functions.

The ratio between $A^p_{\frac{1}{2}}$ for $N\frac{3}{2}^-(1700)$ and that of the second S_{11} resonance $N\frac{1}{2}^-(1650)$ is shown in Fig. 7; note both amplitudes are zero when calculated with unmixed-oscillator wave functions and $H^{\rm nr}$. Once again substantial changes are seen when the wave functions are mixed and when relativistic corrections included in the transition operator, with a larger (and increasing) ratio for the relativized-model calculation. The situation for neutron targets is complicated by electroproduction amplitudes for $N\frac{1}{2}^-(1650)$ [and $N\frac{3}{2}^-(1700)$] which have zeros at Q^2 values between roughly 1.0 and 2.0 GeV^2; accordingly $A^n_{\frac{1}{2}}/A^p_{\frac{1}{2}}$ is plotted in Fig. 8. Proton-target amplitudes for the only other $N=1$ band N^* state, $N\frac{5}{2}^-(1675)D_{15}$, are zero in the SU(6) limit and stay small when mixings and relativistic corrections are applied. The neutron-target asymmetry also remains close to the SU(6) limit of $-\frac{1}{3}$.

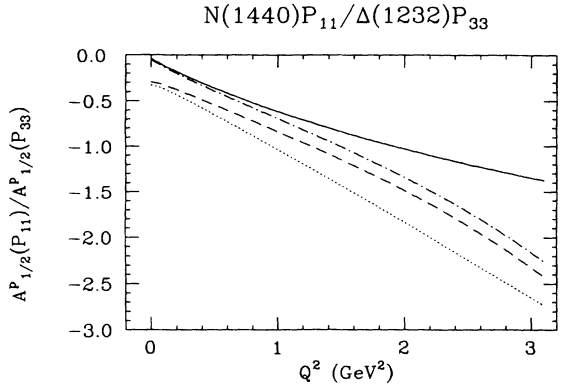

FIG. 12. Ratio of $A^p_{\frac{1}{2}}$ electroproduction amplitudes for $N(1440)P_{11}/\Delta(1232)P_{33}$, calculated in the Breit frame. Legend as in Fig. 4.

Figure 9 shows the helicity asymmetry for the D_{33} resonance $\Delta\frac{3}{2}^-(1700)$ (note that for all Δ states $A^p = A^n$). At the real-photon point $A_{\frac{1}{2}}$ and $A_{\frac{3}{2}}$ are roughly equal, while $A_{\frac{1}{2}}$ dominates at larger Q^2, and all of the calculations give similar results. The ratio between $A_{\frac{1}{2}}$ for the other $N=1$ band Δ resonance, $\Delta\frac{1}{2}^-(1620)S_{31}$, and that of $\Delta\frac{3}{2}^-(1700)$ is shown in Fig. 10; when the wave functions are mixed and when relativistic corrections are added, the $\Delta\frac{1}{2}^-(1620)$ amplitude changes sign at higher Q^2, and is initially larger. Note that the $\Delta\frac{1}{2}^-(1620)$ amplitude is not well predicted at the real-photon point, as can be seen in Table I.

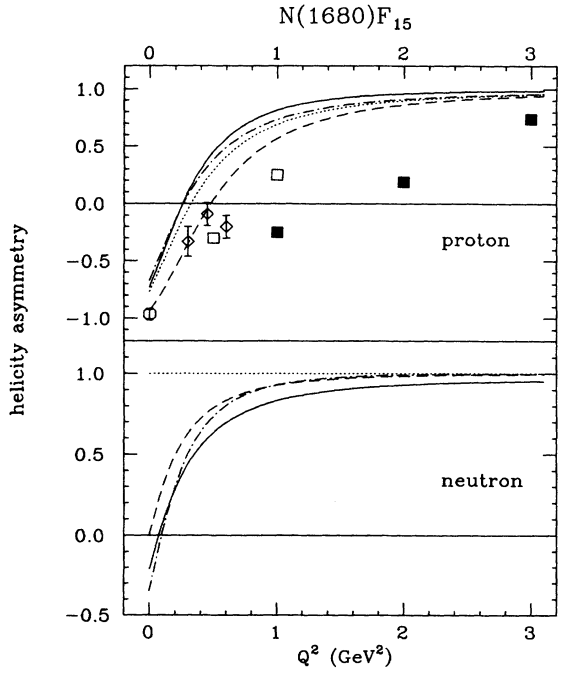

FIG. 11. Proton and neutron-target helicity asymmetries for electroproduction of $N(1680)F_{15}$, calculated in the Breit frame. Legend as in Fig. 4.

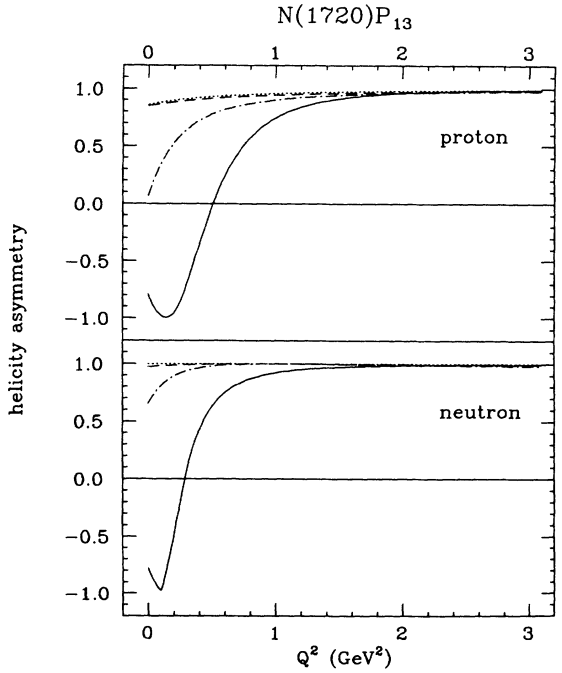

FIG. 13. Proton and neutron-target helicity asymmetries for electroproduction of $N(1720)P_{13}$, calculated in the Breit frame. Legend as in Fig. 4.

C. Positive-parity excited states

The helicity asymmetries of the $N\frac{5}{2}^+(1680)$ are shown in Fig. 11 along with the proton-target data. Hyperfine mixing in the wave functions improves the agreement with the data when $H^{\rm nr}$ is used; however, both calculations using the corrected $H^{\rm em}$ yield too-rapidly changing asymmetries, and also miss the photon-point value. The Close-Li calculation shows better agreement with the data for this ratio; the present calculation (using $H^{\rm em}$ and mixed Isgur-Karl wave functions) is unable to find agreement with their analytic calculation (A_1^M) of the photocouplings of this state, or the helicity asymmetry (calculated, as in Ref. [4], with $\alpha = 0.3$ GeV). The neutron-target amplitudes are roughly equal at the real-photon point, with the $A^n_{\frac{1}{2}}$ amplitude rapidly becoming dominant at higher Q^2. The approach to the SU(6) limit (where $A^n_{\frac{3}{2}} = 0$ and the asymmetry is 1.0) is slower in the relativized-model calculation.

The model predictions for the photocouplings of the Roper resonance $N\frac{1}{2}^+(1440)$ are incompatible [12] with the values from the partial-wave analyses [15]. When we go away from $Q^2 = 0$ the amplitudes are increasing functions; they rapidly reach the SU(6)-limit ratio of $A^n_{\frac{1}{2}}/A^p_{\frac{1}{2}} = -2/3$ (with $A^p_{\frac{1}{2}} > 0$). The ratio between $A^p_{\frac{1}{2}}$ for $N(1440)$ and $\Delta(1232)$ is plotted in Fig. 12; these results imply that if the Roper resonance is a conventional three-quark state, as Q^2 is increased it should eventually be visible in the electroproduction data [42]. This appears to be at odds with the inclusive cross-section data [46], which show no sign of the Roper resonance at modest values of Q^2. The rate at which it increases is, in the relativized model, slower than the roughly linear behavior [1] obtained using unmixed-oscillator wave functions. There are some conflicting results from analyses of the data for the sign of $A^p_{\frac{1}{2}}$ for $N(1440)$ at Q^2 values between 0.5 and 1.0 GeV^2 (see Ref. [42]); better data for the electroproduction of this state will help decide if a conventional explanation of its nature will suffice. The analysis may be complicated by a large width for the Roper [47, 16]. It may be possible that pionic effects are responsible for the discrepancy between the extracted photocouplings of $N(1440)$ [and $\Delta(1232)$] and the quark-model calculation; these effects should disappear when a higher-Q^2 photon is used as a probe.

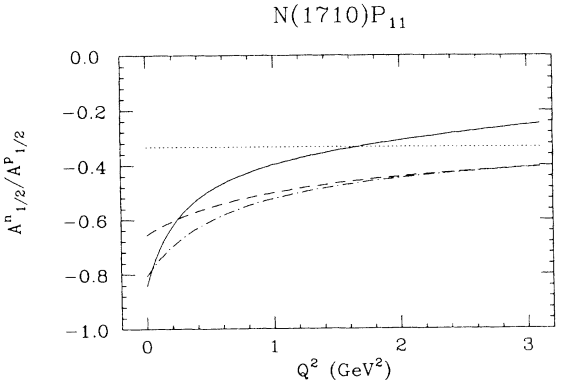

FIG. 14. Ratio $A^n_{\frac{1}{2}}/A^p_{\frac{1}{2}}$ for electroproduction of $N(1710)P_{11}$, calculated in the Breit frame. Legend as in Fig. 4.

Two other low-lying positive-parity excited states which may be accessible at the new experiments are the P_{13} state $N\frac{3}{2}^+(1720)$ and the P_{11} state $N\frac{1}{2}^+(1710)$. The helicity asymmetries for $N\frac{3}{2}^+(1720)$ are shown in Fig. 13; there are substantial changes near $Q^2 = 0$ when the relativistic corrections are added to $H^{\rm nr}$ (see Table II), and the Q^2 dependence is markedly changed in the relativized model. Figure 14 shows $A^n_{\frac{1}{2}}/A^p_{\frac{1}{2}}$ for $N\frac{1}{2}^+(1710)$; the ratio at the photon point (of two rather small photocouplings) is quite different from the SU(6) value of $-\frac{1}{3}$ in the presence of hyperfine mixing, and the trend at higher Q^2 is altered significantly by the adoption of the relativized-model wave functions.

V. CONCLUSIONS

The results of this study confirm the conclusions of Close and Li—that consistently treated relativistic corrections improve the agreement of the electromagnetic couplings with the data—and demonstrate that the use of the relativized model further improves this agreement. This is due in part to the use of a larger effective mass in the relativized-model transition operator, and in part to the more realistic treatment of the wave function and inter-quark potentials in the relativized model. There are also improvements due to the use of an *ab initio* ($^3P_0$) model for the calculation of the strong-decay signs attached to the photocouplings.

One important result of the use of a large basis to expand the wave functions is to remove the strong dependence of the wave function, and the electromagnetic couplings of the state it represents, on the (harmonic-oscillator) size parameter of the basis. It is also confirmed that although, as we have seen above, the components of the $O((p/m)^2)$ relativistic correction may be large, the average expectation value of their sum is considerably smaller than that of the nonrelativistic term. Rather than rely on such (p/m) expansions, the point of view taken here is that Eq. (9) contains a minimum set of tensor terms required by gauge invariance, and so if their coefficients are viewed as free (subject to other constraints like the nucleon magnetic moments) the physics of the transition operator will have been efficiently parametrized.

The result is that the pattern of photocouplings of the nonstrange baryon states is predicted quite well, although with a few notable exceptions. It is significant that the predicted photocouplings of the lightest positive-parity excited states, $\Delta(1232)$, $N(1440)$, $\Delta(1600)$, and $N(1680)$, agree poorly with those extracted from the data. Before giving up on a conventional three-quark assignment for some of these states more should be under-

stood about the extraction of resonance photocouplings from the data, and the effects of virtual baryon-meson loops on the theoretical predictions. Ideally, the analysis of the data and electromagnetic and strong decay models should be linked.

The situation should be greatly improved with the advent of new experiments at MIT/Bates and CEBAF, especially because of their ability to explore in detail these couplings for virtual photons. The results described here for the E_{1+}/M_{1+} ratio in the electromagnetic production of $\Delta(1232)$ imply that nothing can be learned about the quark-quark interactions in these models from studying photoproduction. For electroproduction the results depend strongly on whether nonrelativistic or relativized-model wave functions are used, and are not as sensitive to the relativistic corrections in the transition operator. This calculation shows some improvements in the agreement with the (rather uncertain) electroproduction amplitude ratios for $N(1535)$ and $N(1520)$, and a worsening in the case of $N(1680)$. The model predicts that the couplings of the Roper resonance $N(1440)$ grow relative to those of $\Delta(1232)$, although at a slower rate than was predicted in nonrelativistic models; by $Q^2 = 2$ GeV^2, if it is a radially excited three-quark state, it should couple as strongly as $\Delta(1232)$. This, like the photocouplings, appears to be counter to the experimental situation; however, the Roper resonance may be very broad which would make it difficult to see in electroproduction. There are other low-lying states which have quite model-dependent electroproduction amplitude ratios. The study of these ratios in new experiments would help to determine if the improved fit to the photocouplings found here in the relativized-model calculation also extends to electroproduction.

ACKNOWLEDGMENTS

I wish to thank Zhenping Li for helping motivate this study and for useful discussions, Winston Roberts for his help with calculating signs, and Volker Burkert for useful discussions. This work was supported by the U.S. Department of Energy under Contract No. DE-AC05-84ER40150.

APPENDIX: CALCULATIONAL DETAILS

1. Exchange symmetry

Label the states in the basis described in Sec. II by $\{|\alpha\rangle\}$, where α is a shorthand for the notation $(S_\alpha L_\alpha n_{\rho_\alpha} l_{\rho_\alpha} n_{\lambda_\alpha} l_{\lambda_\alpha})$ (S_α refers to spin wave function type and not only total quark spin). Then to deal with the minimal (12)-exchange symmetry of the basis note that

$$\left\langle \alpha \left| \sum_{i=1}^{3} H_i \right| \beta \right\rangle = \langle \alpha | (H_3 + 2H_2) | \beta \rangle, \tag{A1}$$

where the H_i are defined in analogy to H_3 in Eq. (11). Since $\mathbf{r}_3 = -\sqrt{\frac{2}{3}}\boldsymbol{\lambda} + \mathbf{R}/3$, where $\mathbf{R}$ is the center-of-mass coordinate, evaluation of the H_3 term is simple.

Calculation of the H_2 term becomes simple if the wave functions in this basis are rewritten in terms of a new set $\{|\alpha'\rangle\}$, which have spatial wave functions expressed in terms of $\boldsymbol{\rho}' = (23)\boldsymbol{\rho} = (\mathbf{r}_1 - \mathbf{r}_3)/\sqrt{2}$ and $\boldsymbol{\lambda}' = (23)\boldsymbol{\lambda} = (\mathbf{r}_1 + \mathbf{r}_3 - 2\mathbf{r}_2)/\sqrt{6}$, and the spin wave functions $\chi^{S'} = \chi^S$, $\chi^{\rho'} = (23)\chi^\rho$, and $\chi^{\lambda'} = (23)\chi^\lambda$. Here (23) is the operator which transposes the labels of quarks 2 and 3; note this set is larger than $\{|\alpha\rangle\}$ since we must include both (13)-exchange symmetries. Then

$$\langle \alpha | H_2 | \beta \rangle = \sum_{\alpha', \beta'} \langle \alpha | \alpha' \rangle \langle \alpha' | H_2 | \beta' \rangle \langle \beta' | \beta \rangle, \tag{A2}$$

and the calculation of the matrix element of H_2 in the primed basis is identical to that of H_3 in the usual basis. The problem reduces to the simple one of calculating the overlap matrices $\langle \alpha | \alpha' \rangle$ (one for each basis set with a given J^P).

2. Sample matrix element calculation

As an illustration of the techniques used to calculate the matrix elements of the operators in Eqs. (12), (14), (15), and (16), consider the substate to substate matrix element $\langle \alpha(J,\lambda) | H_{12}^{2b} | \beta(\frac{1}{2}, \lambda - 1) \rangle$ of the two-body operator, needed to form the helicity amplitude A_λ^N for the electromagnetic excitation of a resonance with total spin J from a nucleon. The states $|\alpha(J,\lambda)\rangle$ and $|\beta(\frac{1}{2}, \lambda - 1)\rangle$ are elements of the bases described above with specific $|JM\rangle$ values and parities. In particular focus on one part of H_{12}^{2b}, that proportional to $(\sigma_{\lambda z}/2) p_{\lambda +} \exp(-ik\sqrt{\frac{2}{3}}\lambda_z)$. Then

$$\begin{aligned}
&\langle \alpha(J,\lambda) | \frac{\sigma_{\lambda z}}{2} p_{\lambda +} e^{-ik\sqrt{\frac{2}{3}}\lambda_z} | \beta(\tfrac{1}{2}, \lambda - 1) \rangle \\
&\quad = C(L_\alpha, S_\alpha, M, \lambda - M; J, \lambda) C(L_\beta, S_\beta, M - 1, \lambda - M; \tfrac{1}{2}, \lambda - 1) C(S_\beta, 1, \lambda - M, 0; S_\alpha, \lambda - M) \\
&\qquad \times \langle S_\alpha || \frac{\boldsymbol{\sigma}_\lambda}{2} || S_\beta \rangle \langle \psi_{L_\alpha M n_{\rho_\alpha} l_{\rho_\alpha} n_{\lambda_\alpha} l_{\lambda_\alpha}} | p_{\lambda +} e^{-ik\sqrt{\frac{2}{3}}\lambda_z} | \psi_{L_\beta M - 1 n_{\rho_\beta} l_{\rho_\beta} n_{\lambda_\beta} l_{\lambda_\beta}} \rangle,
\end{aligned} \tag{A3}$$

where the reduced matrix elements of $\boldsymbol{\sigma}_\lambda/2$ are listed below. The spatial wave functions are then expanded using Eq. (6), and orthogonality in the $\boldsymbol{\rho}$ oscillator invoked to reduce the result to a $\boldsymbol{\lambda}$-oscillator expectation value. This can be further reduced by insertion of a complete set of $\boldsymbol{\lambda}$-oscillator spatial wave functions $\sum_{n_\gamma,l_\gamma}|n_\gamma\, l_\gamma\, m\rangle\langle n_\gamma\, l_\gamma\, m| \equiv 1$, with the result that the spatial matrix element in Eq. (A3) can be written in terms of products of various Clebsch-Gordan coefficients, the reduced matrix elements of $\mathbf{p}_\lambda$, and the matrix elements of the phase $\exp(-ik\sqrt{\frac{2}{3}}\lambda_z)$. These reduced matrix elements are also listed below.

3. Reduced matrix elements

To form the matrix elements of the operators in Eqs. (12), (14), (15), and (16) the values of the reduced matrix elements of the quark-spin operators $\boldsymbol{\sigma}_3/2$, $\boldsymbol{\sigma}_\rho/2$, and $\boldsymbol{\sigma}_\lambda/2$ are needed. With rows and columns in the order $\chi^S_{\frac{3}{2}}$, $\chi^\rho_{\frac{1}{2}}$, and $\chi^\lambda_{\frac{1}{2}}$ we have

$$\langle S_\alpha||\frac{\boldsymbol{\sigma}_3}{2}||S_\beta\rangle = \frac{\sqrt{3}}{6}\begin{bmatrix}\sqrt{5} & 0 & -2\\ 0 & 3 & 0\\ 2\sqrt{2} & 0 & -1\end{bmatrix}, \tag{A4}$$

where the rows correspond to S_α values, the columns to S_β. Similarly we have

$$\langle S_\alpha||\frac{\boldsymbol{\sigma}_\rho}{2}||S_\beta\rangle = \frac{1}{\sqrt{2}}\langle S_\alpha||\frac{\boldsymbol{\sigma}_1-\boldsymbol{\sigma}_2}{2}||S_\beta\rangle = \frac{\sqrt{2}}{2}\begin{bmatrix}0 & 1 & 0\\ -\sqrt{2} & 0 & -1\\ 0 & -1 & 0\end{bmatrix}, \tag{A5}$$

and

$$\langle S_\alpha||\frac{\boldsymbol{\sigma}_\lambda}{2}||S_\beta\rangle = \frac{1}{\sqrt{6}}\langle S_\alpha||\frac{\boldsymbol{\sigma}_1+\boldsymbol{\sigma}_2-2\boldsymbol{\sigma}_3}{2}||S_\beta\rangle = \frac{\sqrt{2}}{2}\begin{bmatrix}0 & 0 & 1\\ 0 & -1 & 0\\ -\sqrt{2} & 0 & 1\end{bmatrix}. \tag{A6}$$

Also required are the reduced matrix elements of the operators $\mathbf{p}_\rho$ and $\mathbf{p}_\lambda$ between $\boldsymbol{\rho}$- and $\boldsymbol{\lambda}$-oscillator wave functions, respectively. These are

$$\langle n_{\rho_\alpha}\, l_{\rho_\alpha}||\mathbf{p}_\rho||n_{\rho_\beta}\, l_{\rho_\beta}\rangle = i\alpha C(l_{\rho_\alpha},1,0,0;l_{\rho_\beta},0)\langle n_{\rho_\alpha}\, l_{\rho_\alpha}|\frac{ip}{\alpha}|n_{\rho_\beta}\, l_{\rho_\beta}\rangle \tag{A7}$$

(and similarly for $\langle n_{\lambda_\alpha}\, l_{\lambda_\alpha}||\mathbf{p}_\lambda||n_{\lambda_\beta}\, l_{\rho_\beta}\rangle$); here $\langle n\, l|ip/\alpha|n'\, l'\rangle$ is a radial integral which is nonzero only when $l' = l-1$, where it takes the values

$$\langle n\, l|i\frac{p}{\alpha}|n'\, l-1\rangle = \begin{cases}-\sqrt{n+l+\frac{1}{2}} & \text{if} \quad n'=n,\\ -\sqrt{n+1} & \text{if} \quad n'=n+1,\end{cases} \tag{A8}$$

and when $l' = l+1$, where

$$\langle n\, l|i\frac{p}{\alpha}|n'\, l+1\rangle = \begin{cases}\sqrt{n} & \text{if} \quad n'=n-1,\\ \sqrt{n+l+\frac{3}{2}} & \text{if} \quad n'=n.\end{cases} \tag{A9}$$

The various transition operators are also proportional to the phase factor $\exp(-ik\sqrt{\frac{2}{3}}\lambda_z)$, whose $\boldsymbol{\lambda}$-oscillator expectation values are

$$\langle n_{\lambda_\alpha}\, l_{\lambda_\alpha}\, m|e^{-ik\sqrt{\frac{2}{3}}\lambda_z}|n_{\lambda_\beta}\, l_{\lambda_\beta}\, m\rangle = \sum_{K=|l_{\lambda_\alpha}-l_{\lambda_\beta}|}^{l_{\lambda_\alpha}+l_{\lambda_\beta}}(2K+1)C(l_{\lambda_\beta},K,m,0;l_{\lambda_\alpha},m)\sqrt{\frac{2l_{\lambda_\beta}+1}{2l_{\lambda_\alpha+1}}} \times C(K,l_{\lambda_\beta},0,0;l_{\lambda_\alpha},0)\langle n_{\lambda_\alpha}\, l_{\lambda_\alpha}|\left\{\frac{z^K d^K}{(zdz)^K}\left[\frac{\sinh z}{z}\right]\right\}_{z=-ik\sqrt{\frac{2}{3}}\lambda}|n_{\lambda_\beta}\, l_{\lambda_\beta}\rangle, \tag{A10}$$

where the last factor is a radial integral, with

$$\langle n_{\lambda_\alpha}\, l_{\lambda_\alpha}|f(\lambda)|n_{\lambda_\beta}\, l_{\lambda_\beta}\rangle = \mathcal{N}_{n_{\lambda_\alpha} l_{\lambda_\alpha}}\mathcal{N}_{n_{\lambda_\beta} l_{\lambda_\beta}}\int_0^\infty d(\alpha\lambda)(\alpha\lambda)^{2+l_{\lambda_\alpha}+l_{\lambda_\beta}}e^{-\alpha^2\lambda^2}L_{n_{\lambda_\beta}}^{l_{\lambda_\beta}+\frac{1}{2}}(\alpha^2\lambda^2)f(\lambda)L_{n_{\lambda_\alpha}}^{l_{\lambda_\alpha}+\frac{1}{2}}(\alpha^2\lambda^2). \tag{A11}$$

Note that K is restricted to even (the radial integral is real) or odd (the radial integral is pure imaginary) values by the parity rule for the second Clebsch-Gordan coefficient.

[1] L.A. Copley, G. Karl, and E. Obryk, Nucl. Phys. **B13**, 303 (1969).

[2] R.P. Feynman, M. Kislinger, and F. Ravndal, Phys. Rev. D **3**, 2706 (1971).

[3] R. Koniuk and N. Isgur, Phys. Rev. D **21**, 1868 (1980).

[4] F.E. Close and Zhenping Li, Phys. Rev. D **42**, 2194 (1990); Zhenping Li and F.E. Close, *ibid.* **42**, 2207 (1990).

[5] M. Warns, H. Schröder, W.P. Pfeil, and H. Rollnik, Z. Phys. C **45**, 613 (1990); **45**, 627 (1990); M. Warns, W. Pfeil, and H. Rollnik, Phys. Rev. D **42**, 2215 (1990).

[6] T. Kubota and K. Ohta, Phys. Lett. **65B**, 374 (1976).

[7] R. Sartor and Fl. Stancu, Phys. Rev. D **31**, 128 (1985); **33**, 727 (1986).

[8] C.P. Forsyth and R.E. Cutkosky, Phys. Rev. Lett. **46**,

576 (1981); Z. Phys. C **18**, 219 (1983); C.P. Forsyth, Ph.D. thesis, Carnegie Mellon University, 1981.
[9] N. Isgur and G. Karl, Phys. Lett. **72B**, 109 (1977); **74B**, 353 (1978); Phys. Rev. D **18**, 4187 (1978).
[10] N. Isgur and G. Karl, Phys. Rev. D **19**, 2653 (1979).
[11] N. Isgur, G. Karl, and R. Koniuk, Phys. Rev. Lett. **41**, 1269 (1978); Phys. Rev. D **25**, 2394 (1982).
[12] S. Capstick, Phys. Rev. D **46**, 1965 (1992).
[13] S. Godfrey and N. Isgur, Phys. Rev. D **32**, 189 (1985).
[14] S. Capstick and N. Isgur, Phys. Rev. D **34**, 2809 (1986).
[15] Particle Data Group, J.J. Hernández *et al.*, Phys. Lett. B **239**, 1 (1990).
[16] S. Capstick and W. Roberts, CEBAF Report No. CEBAF-TH-92-05 (unpublished).
[17] N. Isgur, in *Proceedings of the CEBAF/SURA 1984 Summer Workshop*, Newport News, Virginia, 1984, edited by F. Gross and R.R. Whitney (CEBAF, Newport News, 1984).
[18] C. Hayne and N. Isgur, Phys. Rev. D **25**, 1944 (1982).
[19] F. Foster and G. Hughes, Z. Phys. C **14**, 123 (1982).
[20] F.E. Close and F.J. Gilman, Phys. Lett. **38B**, 514 (1972).
[21] S. Ono, Nucl. Phys. **B107**, 522 (1976).
[22] S.S. Gershtein and G.V. Dzhikiya, Yad. Fiz. **34**, 1566 (1981) [Sov. J. Nucl. Phys. **34**, 870 (1981)]; Isgur, Karl, and Koniuk [11]; M. Weyrauch and H.J. Weber, Phys. Lett. B **171**, 13 (1986); M. Bourdeau and N.C. Mukhopadhyay, Phys. Rev. Lett. **58**, 976 (1987); S.A. Gogilidze, Yu.S. Surovtsev, and F.G. Tkebuchava, Yad. Fiz. **45**, 1085 (1987) [Sov. J. Nucl. Phys. **45**, 674 (1987)]; see also references in Ref. [24].
[23] For a review of the experimental and theoretical situations see N.C. Mukhopadhyay, in *Excited Baryons 1988*, Proceedings of the Topical Workshop, Troy, New York, 1988, edited by G. Adams, N. Mukhopadhyay, and P. Stoler (World Scientific, Singapore, 1989), p. 205; C.N. Papanicolas, *ibid.*, p. 235; V. Burkert, in *The Hadron Mass Spectrum*, Proceedings of the Conference, St. Goar, Germany, 1990, edited by E. Klempt and K. Peters [Nucl. Phys. B (Proc. Suppl.) **21**, 287 (1991)].
[24] S. Capstick and G. Karl, Phys. Rev. D **41**, 2767 (1990).
[25] H.G. Dosch and V. Müller, Nucl. Phys. **B116**, 470 (1976); R.E. Cutkosky and R.E. Hendrick, Phys. Rev. D **16**, 786 (1977); **16**, 793 (1977); J. Carlson, J.B. Kogut, and V.R. Pandharipande, *ibid.* **27**, 233 (1983); **28**, 2807 (1983).
[26] In Ref. [14] the $J^P = \frac{1}{2}^+$ states were expanded to $N = 8$; however, in decay calculations it is preferable to have the initial and final states expanded to the same level, and there is little change in the energies of these states in going from $N = 6$ to $N = 8$.
[27] A good fit to the baryon spectrum was obtained in Ref. [14] with all of the parameters the same as in the meson physics calculation of Ref. [13]. Our *best* fit used a string tension which was reduced 15% from the meson value.
[28] S.J. Brodsky and J. Primack, Ann. Phys. (N.Y.) **52**, 315 (1969); F.E. Close and L.A. Copley, Nucl. Phys. **B19**, 477 (1970); F.E. Close and H. Osborn, Phys. Rev. D **2**, 2127 (1970); R. Faustov, Nuovo Cimento **69A**, 37 (1970); G. Feinberg and J. Sucher, Phys. Rev. Lett. **35**, 1740 (1975); J. Sucher, Rep. Prog. Phys. **41**, 1781 (1978).
[29] K. Ohta, Phys. Rev. Lett. **43**, 1201 (1979).
[30] R. McClary and N. Byers, Phys. Rev. D **28**, 1692 (1983).
[31] A theoretical error of 20, in units of 10^{-3} GeV$^{-\frac{1}{2}}$, is added in quadrature with the experimental errors quoted in the Particle Data Group summary [15] for each photocoupling amplitude; χ^2 is then formed by summing over all (forty-six) measured photocouplings.
[32] Raising the quark mass more than roughly thirty percent from the nonrelativistic value results in only minor reductions in χ^2. Because of the generally small size of the two-body terms, changes in M_T have little effect on the fit.
[33] I. Guiasu and R. Koniuk, Phys. Rev. D **36**, 2757 (1987).
[34] R.M. Davidson and N.C. Mukhopadhyay, Phys. Rev. D **42**, 20 (1990); R.M. Davidson, N.C. Mukhopadhyay, and R.S. Wittman, *ibid.* **43**, 71 (1991); T.-S. Harry Lee (private communication).
[35] N. Awaji and R. Kajikawa, in *Lepton and Photon Interactions at High Energies*, Proceedings of the 10th International Symposium, Bonn, Germany, 1981, edited by W. Pfeil (Physikalisches Institut, Bonn University, Bonn, 1981); H. Fujii *et al.*, Nucl. Phys. **B197**, 365 (1982).
[36] R.C.E. Devenish, D.H. Lyth, and W.A. Rankin, Phys. Lett. **52B**, 227 (1974).
[37] R.L. Crawford, in *Baryon 1980*, Proceedings of the 4th International Conference on Baryon Resonances, Toronto, Canada, 1980, edited by N. Isgur (University of Toronto, Toronto, 1980).
[38] I.M. Barbour, R.L. Crawford, and N.H. Parsons, Nucl. Phys. **B141**, 253 (1978).
[39] R.L. Crawford and W.T. Morton, Nucl. Phys. **B211**, 1 (1983).
[40] Here and in what follows we have used $\alpha = 0.41$ GeV when calculating with the Isgur-Karl model wave functions, which is the value used by Koniuk and Isgur in their fit to the photocouplings [3] and by Close and Li in their A^1_M photocouplings calculation [4], and is compatible with the spectroscopy in this model.
[41] Isgur, Karl, and Koniuk [11]; note that a definition of the multipoles which differs from the usual one was adopted, i.e., $E = (A_{\frac{3}{2}} - \sqrt{3}A_{\frac{1}{2}})/2$, $M = (\sqrt{3}A_{\frac{3}{2}} + A_{\frac{1}{2}})/2$, so that their ratio E/M is $-\sqrt{3}E_{1+}/M_{1+}$.
[42] V. Burkert, in *Excited Baryons 1988* [23], p. 122; in *Nucleon Resonances and Nucleon Structure*, edited by G. Miller (World Scientific, Singapore, in press).
[43] H. Breuker *et al.*, Z. Phys. C **13**, 113 (1982); **17**, 121 (1983).
[44] E. Evangelides *et al.*, Nucl. Phys. **B71**, 381 (1974).
[45] W. Brasse *et al.*, Nucl. Phys. **B110**, 410 (1976); **B139**, 37 (1978); V. Gerhardt, Int. Report No. DESY-F21-79/02, 1979 (unpublished); R. Haidan, Int. Report No. DESY-F21-79/03, 1979 (unpublished).
[46] P. Stoler, Phys. Rev. D **44**, 73 (1991).
[47] R.E. Cutkosky and S. Wang, Phys. Rev. D **42**, 235 (1990).